Supporting Information for:

Robust future intensification of winter precipitation over the United States

Akintomide A. Akinsanola[1,2], Ziming Chen[3], Gabriel J. Kooperman[4], and Vishal Bobde[1]

[1]Department of Earth and Environmental Sciences, University of Illinois Chicago, Chicago, IL, USA

[2]Environmental Science Division, Argonne National Laboratory, Lemont, IL, USA

[3] Atmospheric, Climate, & Earth Sciences (ACES) Division, Pacific Northwest National Laboratory, Richland, Washington, USA

[4]Department of Geography, University of Georgia, Athens, GA, USA

*Corresponding author: *Akintomide Afolayan Akinsanola (aakinsan@uic.edu)*

Text S1. Method for separating the sources of uncertainty

Following refs.[1,2], the uncertainty arising from internal variability, model and scenarios is separated as follows:

1. The precipitation simulation of each individual model is fitted using ordinary least squares with a fourth-order polynomial over 1950-2100. The raw simulations $X_{m,s,t}$ for each model *m*, scenario *s*, and year *t* is expressed as

$$X_{m,s,t} = x_{m,s,t} + i_{m,s} + \varepsilon_{m,s,t} \qquad 1$$

where the smooth fit is denoted as $x_{m,s,t}$, the reference precipitation is denoted as $i_{m,s}$ and the residual $\varepsilon_{m,s,t}$ refers to internal variability. The reference precipitation is the climatology of 1985 to 2014.

2. The internal variability is estimated from the multimodel mean of the variance of residuals across scenarios (i.e., SSP2–4.5, SSP3–7.0, and SSP5–8.5) and time:

$$V = \frac{1}{N_m} \sum_m var_{s,t}\left(\varepsilon_{m,s,t}\right) \qquad 2$$

where $\mathrm{var}_{s,t}\left(\varepsilon_{m,s,t}\right)$ denotes the variance across scenarios and time for the model m, and N_m is the number of models.

3. The model uncertainty is defined as multi-scenario mean of the variance of smooth fit across models

$$M(t) = \frac{1}{N_s} \sum_s var_m(x_{m,s,t}) \qquad 3$$

where N_s represents the number of scenarios.

4. The scenario uncertainty is defined as the variance of multimodel and multi-scenario mean smooth fit,

$$S(t) = var_s\left(\frac{1}{N_m} \sum_m x_{m,s,t}\right) \qquad 4$$

5. Assuming model uncertainty, scenario uncertainty, and internal variability are independent of each other, the total uncertainty can be expressed as:

$$T(t) = V + S(t) + M(t) \qquad 5$$

6. The mean change of precipitation of all models and scenarios is defined as the average of models and scenarios relative to the reference period,

$$G(t) = \frac{1}{N_s}\frac{1}{N_m}\sum_{m,s} x_{m,s,t} \qquad 6$$

7. The fraction of total variance explained by the three components is defined as the ratio of model uncertainty M*(t)*, scenario uncertainty S*(t)* and internal variability V to total uncertainty T*(t)*.

Table S1. Information for the nineteen CMIP6 climate models used in this study.

S/N	Model	Short name	Institute	Resolution (^{o}lon × ^{o}lat)	References
1	ACCESS-CM2	ACM2	Commonwealth Scientific and Industrial Research Organisation	1.88×1.25	Dix et al (2019)[3-6]
2	ACCESS-ESM1-5	AESM	Commonwealth Scientific and Industrial Research Organisation	1.88×1.24	Ziehn et al (2019)[7-10]
3	AWI-CM-1-1-MR	AWI	Alfred Wegener Institute Helmholtz Centre for Polar and Marine Research	1.5x1.5	Semmler et al (2018)[11,12], Semmler et al (2019)[13,14]
4	BCC-CSM2-MR	BCC	Beijing Climate Center (BCC) and China Meteorological Administration (CMA)	1.13×1.13	Wu *et al* (2018)[15], Xin et al (2019)[17-18]
5	CAMS-CSM1-0	CAMS	Chinese Academy of Meteorological Sciences	1.12x1.12	Rong (2019)[19-22]
6	CanESM5	Can5	Canadian Earth System Model	2.81×2.81	Swart *et al* (2019)[23-26]
7	CMCC-CM2-SR5	CMCC	Euro-Mediterranean Centre on Climate Change coupled climate model	1.25×0.94	Lovato & Peano (2020)[27-30]
8	EC-Earth3	E3	EC-EARTH consortium	0.70×0.70	EC-Earth (2019)[31-34]
9	EC-Earth3-Veg	E3V	EC-EARTH consortium	0.70×0.70	EC-Earth (2019)[35-38]
10	INM-CM4-8	INM4	Institute of Numerical Mathematics	2.00×1.50	Volodin et al (2019)[39-42]
11	INM-CM5-0	INM5	Institute of Numerical Mathematics	2.00×1.50	Volodin et al (2019)[43-46]
12	IPSL-CM6A-LR	IPSL	Institute Pierre-Simon Laplace (IPSL)	2.50×1.26	Boucher *et al* (2018)[47], Boucher et al (2019)[48-50]
13	MIROC6	MIRO	Japanese Modeling Community	1.41×1.41	Tatebe and Watanabe (2018)[51], Shiogama et al (2019)[52-54]
14	MPI-ESM1-2-HR	MPIH	Max Planck Institute	0.94×0.94	Jungclaus et al (2019)[55], Schupfner et al (2019)[56-58]
15	MPI-ESM1-2-LR	MPIL	Max Planck Institute	1.88×1.88	Wieners et al (2019)[59-62]
16	MRI-ESM2-0	MRI	Meteorological Research Institute (MRI)	1.13×1.13	Yukimoto et al (2019)[63-66]
17	NorESM2-LM	NorL	Norwegian Earth System Model	2.5x1.9	Seland et al (2019)[67-70]
18	NorESM2-MM	NorM	Norwegian Earth System Model	1.25×0.94	Bentsen et al (2019)[71-74]
19	TaiESM1	TESM	Taiwan Earth System Model	1.25 × 0.94	Lee & Liang (2020)[75-78]

Table S2. Contribution from changes in the vertical velocity anomaly and humidity anomaly to precipitation changes. Intermodel correlation of precipitation changes (P') with vertical velocity at 500 hPa (ω'_{500}) and precipitable water changes (q').

U.S. & Subregions	P' (%/K) & ω'_{500} (Pa/s)	P' & q' (%/K)
US	–0.41 ($p < 0.08$)	0.31 ($p < 0.20$)
NW	–0.76 ($p < 0.001$)	–0.03 ($p < 0.89$)
SW	–0.68 ($p < 0.001$)	0.45 ($p < 0.06$)
NGP	–0.47 ($p < 0.04$)	0.33 ($p < 0.16$)
SGP	–0.57 ($p < 0.01$)	0.27 ($p < 0.26$)
MW	–0.31 ($p < 0.20$)	0.38 ($p < 0.11$)
SE	–0.40 ($p < 0.09$)	0.14 ($p < 0.58$)
NE	–0.38 ($p < 0.11$)	0.57 ($p < 0.01$)

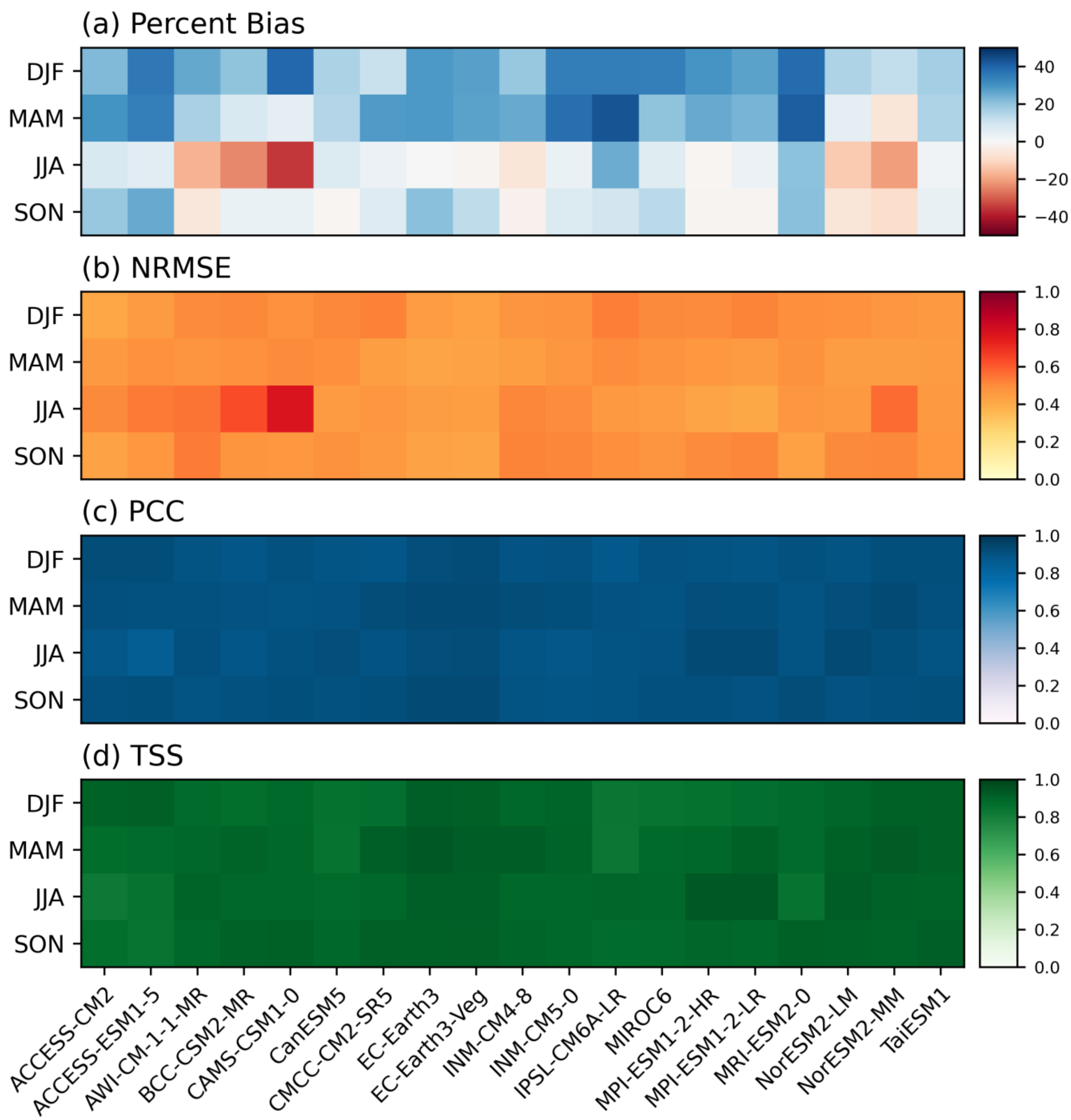

Figure S1. Portrait diagrams showing the percentage bias (a), normalized root mean square error (b), pattern correlation coefficient (c), and Taylor skill score (d) between CRU and all CMIP6 models.

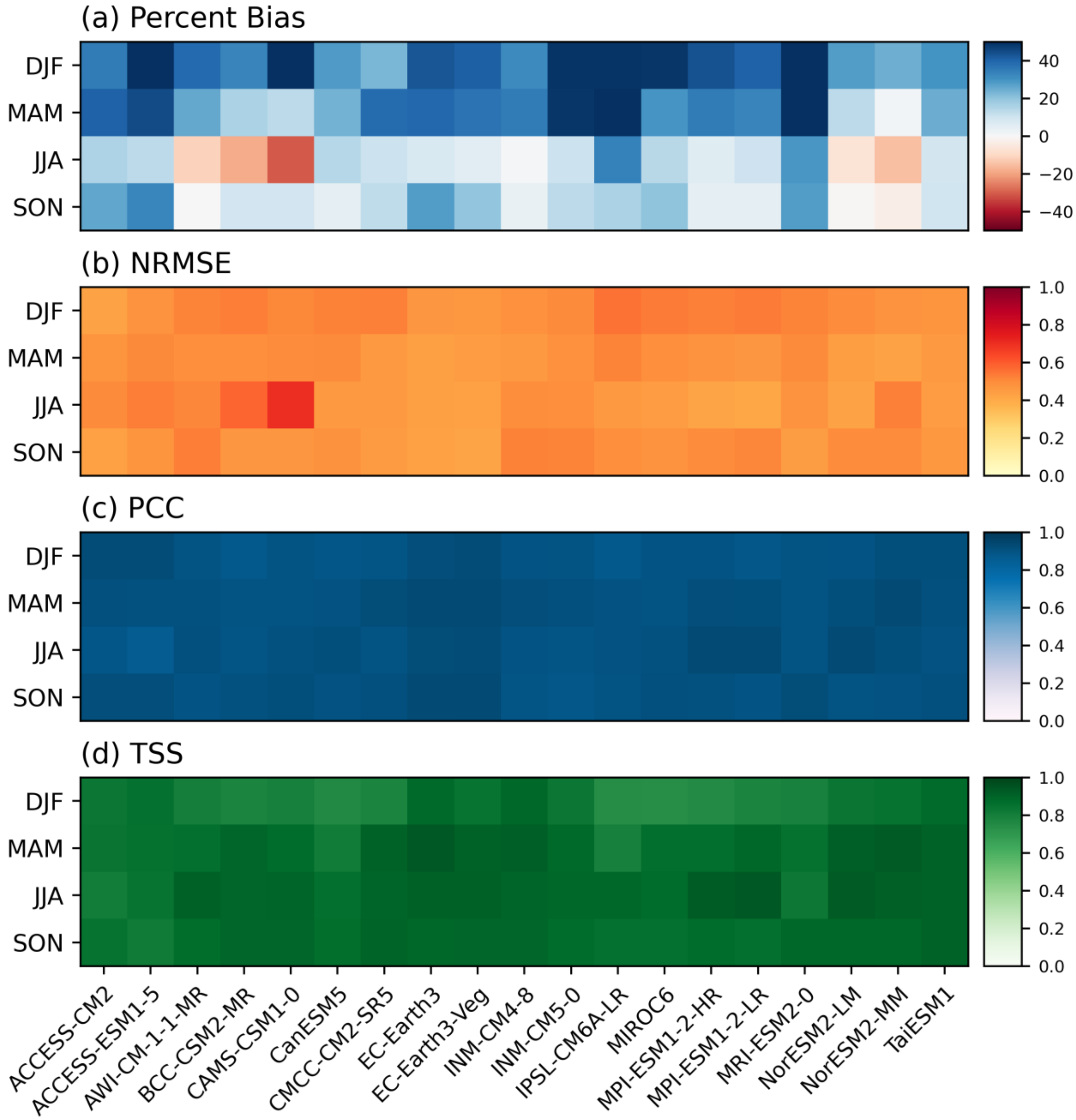

Figure S2. Portrait diagrams showing the percentage bias (a), normalized root mean square error (b), pattern correlation coefficient (c), and Taylor skill score (d) between GPCC and all CMIP6 models.

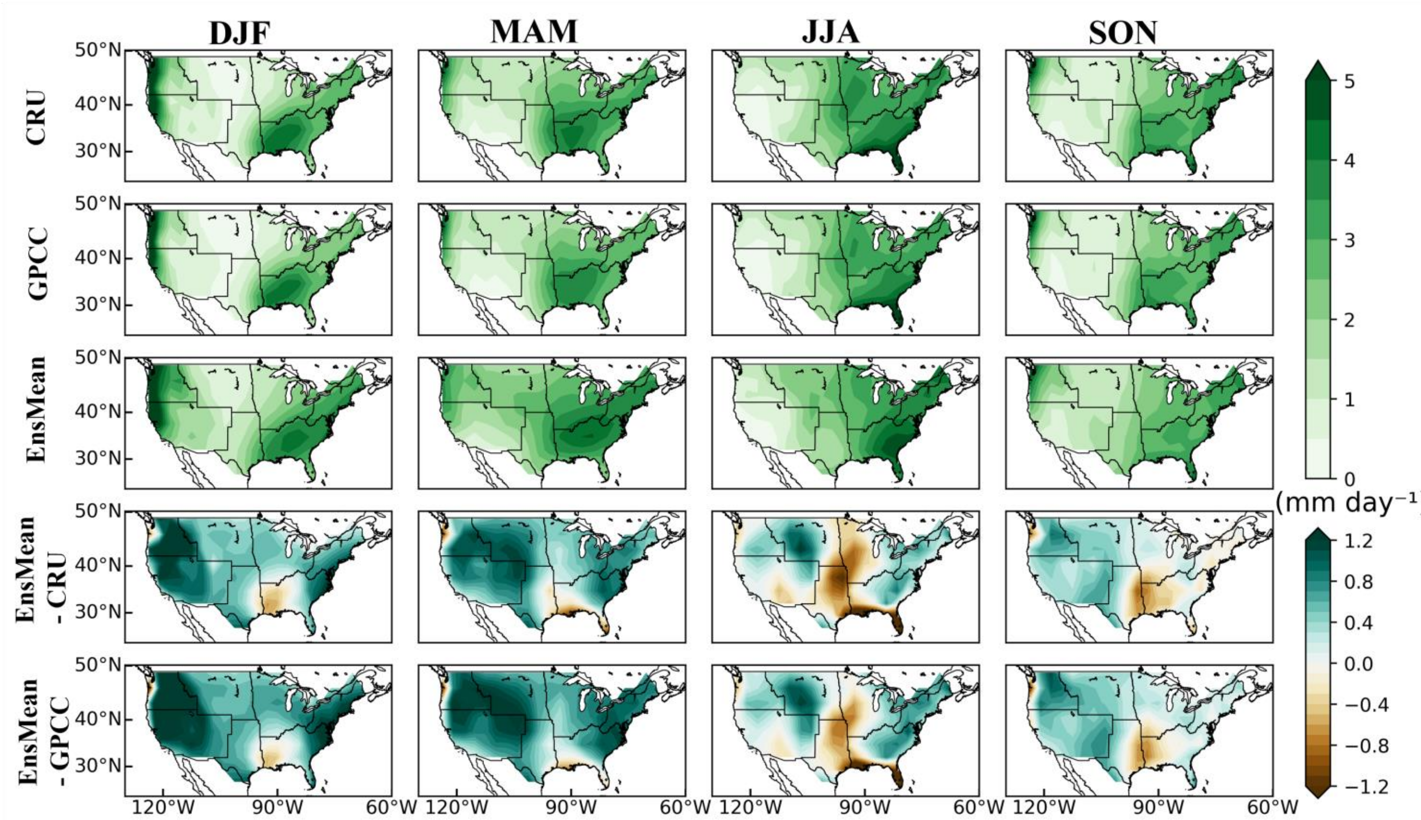

Figure S3. (left)–(right) Spatial distribution of mean precipitation for DJF, MAM, JJA, and SON seasons from (top)–(bottom) CRU, GPCC, EnsMean, bias of EnsMean relative to CRU, and bias of EnsMean relative to GPCC over the present-day period, 1985–2014. Unit: mm day^{-1}.

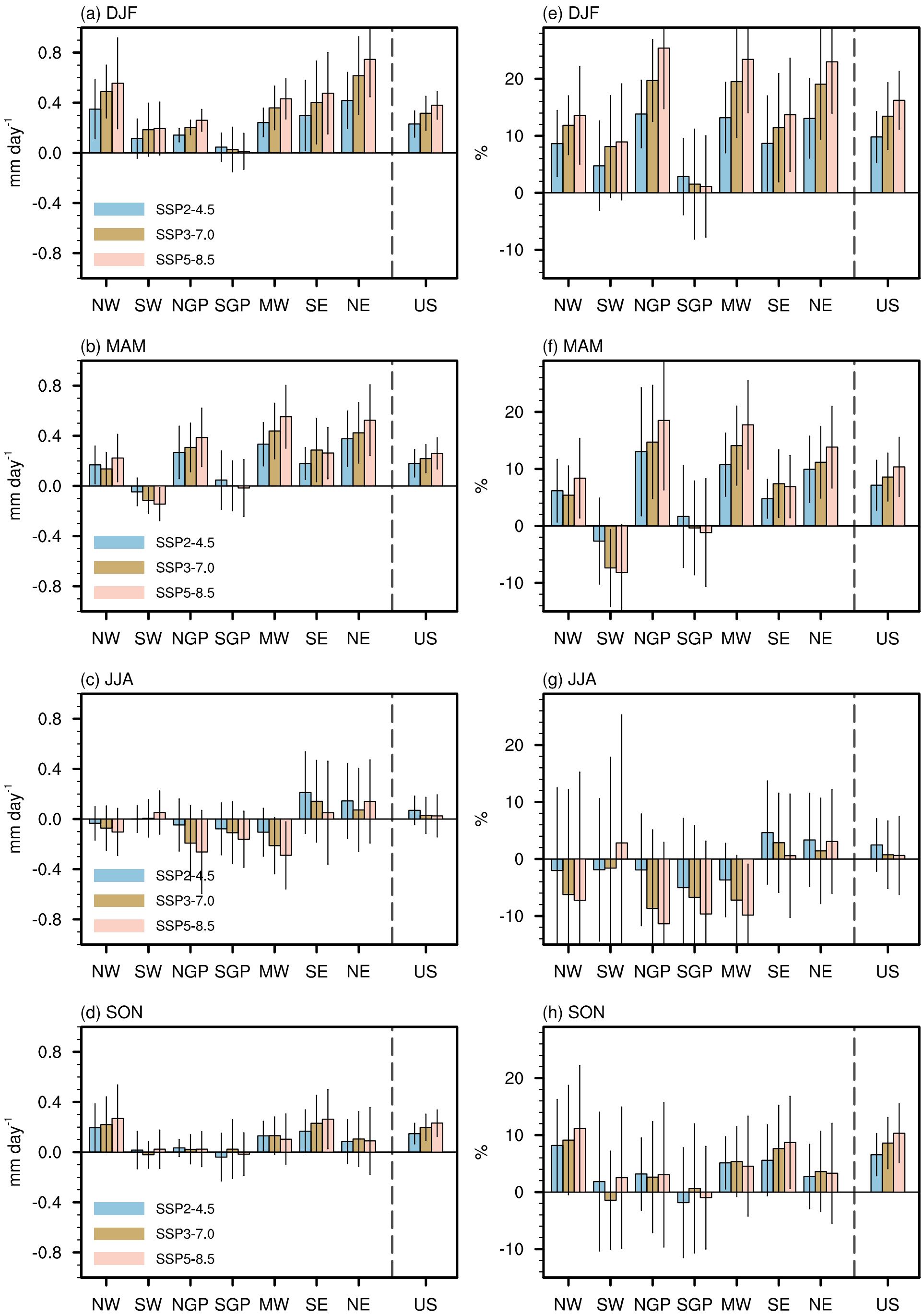

Figure S4. Projected area-weighted subregional changes in seasonal precipitation (2070–2099 relative to 1985–2014). (a to d) show absolute value of projected changes (unit: mm day^{-1}), while (e to h) show percentage changes relative to 1985–2014 (unit: %). Bars are the multimodel ensemble mean (EnsMean) values, while the vertical line denotes the plus/minus one-time STD, which is based on the spread across models. Figures are computed as the absolute/percentage change in the regional weighted average (NW-Northwest, SW-Southwest, NGP-Northern Great Plains, SGP- Southern Great Plains, MW-Midwest, SE-Southeast, NE-Northeast, US-all of US).

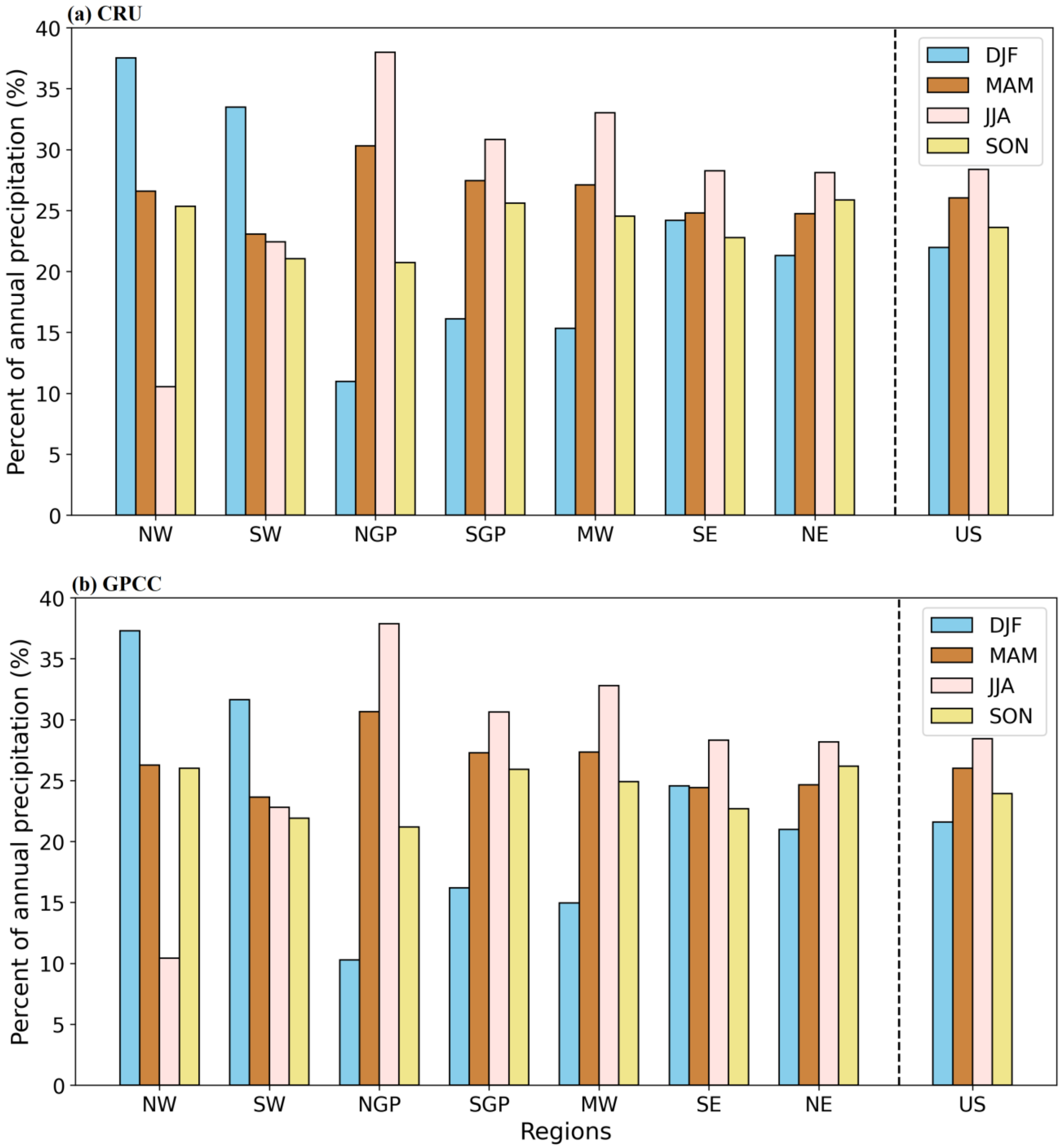

Figure S5. Percentage contribution of seasonal precipitation to the annual total from (a) CRU and (b) GPCC for the period 1985-2014 across the U.S. and its subregions.

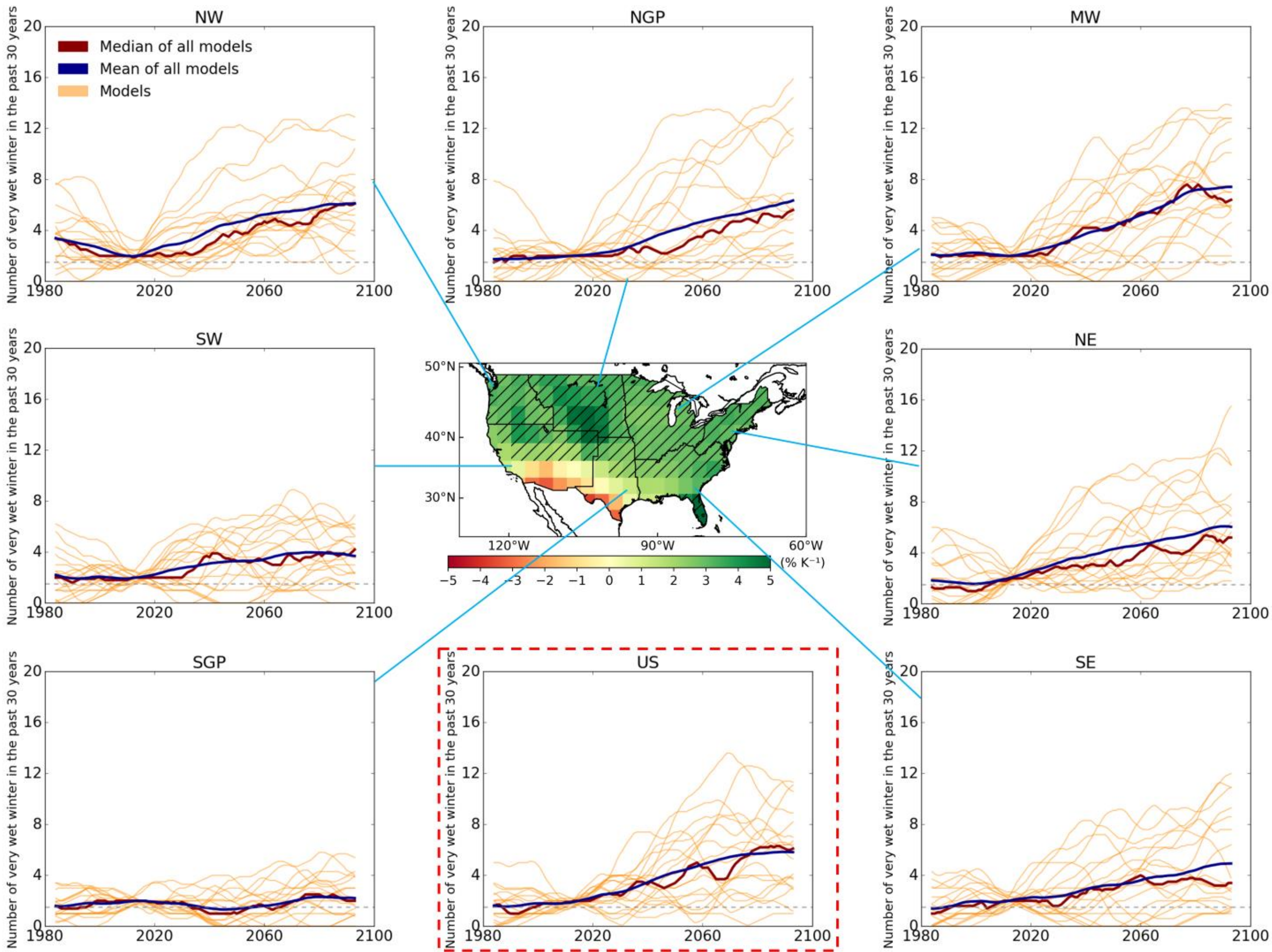

Figure S6. Projected changes in winter precipitation (2070–2099 relative to 1985–2014) under SSP2–4.5. Spatial change in winter precipitation over the US scaled with mean temperature change (% K^{-1}; center figure). Hatching indicates grid points where at least 70% of the models agree on the sign of the EnsMean change. Time evolution of the number of wet winter years over different regions under SSP2–4.5 (time series plots). The number of wet years in the preceding 30 years is plotted and smoothed using 10-year running means. Red (blue) lines represent the multimodel ensemble median (EnsMean). Orange lines represent individual model results. The horizontal dotted gray line marks the reference of 1.5 out of 30 winter wet years based on the 95th percentile value in the historical period (1985–2014).

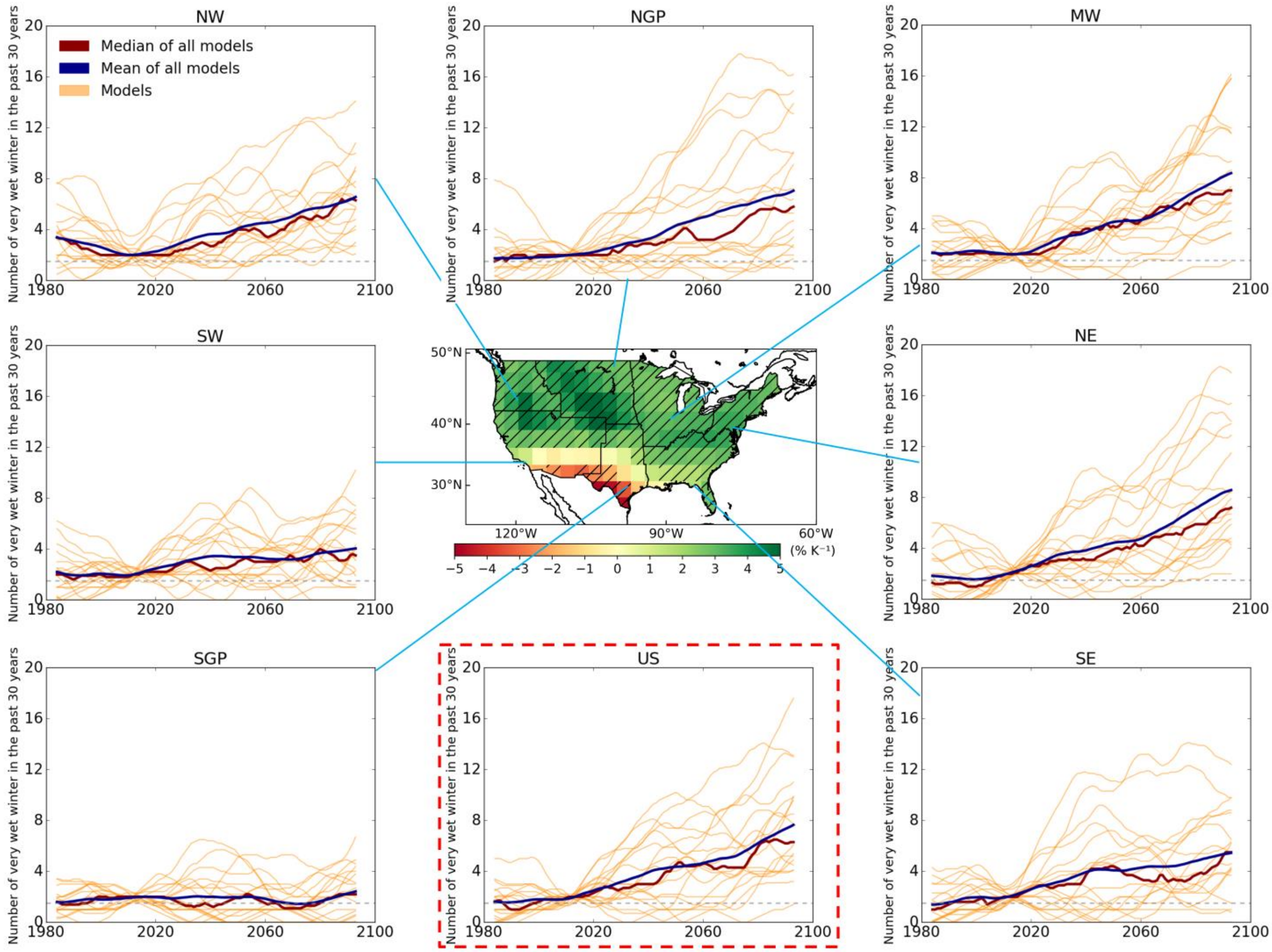

Figure S7. Projected changes in winter precipitation (2070–2099 relative to 1985–2014) under SSP3–7.0. Spatial change in winter precipitation over the US scaled with mean temperature change (% K^{-1}; center figure). Hatching indicates grid points where at least 70% of the models agree on the sign of the EnsMean change. Time evolution of the number of wet winter years over different regions under SSP3–7.0. (time series plots). The number of wet years in the preceding 30 years is plotted and smoothed using 10-year running means. Red (blue) lines represent the multimodel ensemble median (EnsMean). Orange lines represent individual model results. The horizontal dotted gray line marks the reference of 1.5 out of 30 winter wet years based on the 95th percentile value in the historical period (1985–2014).

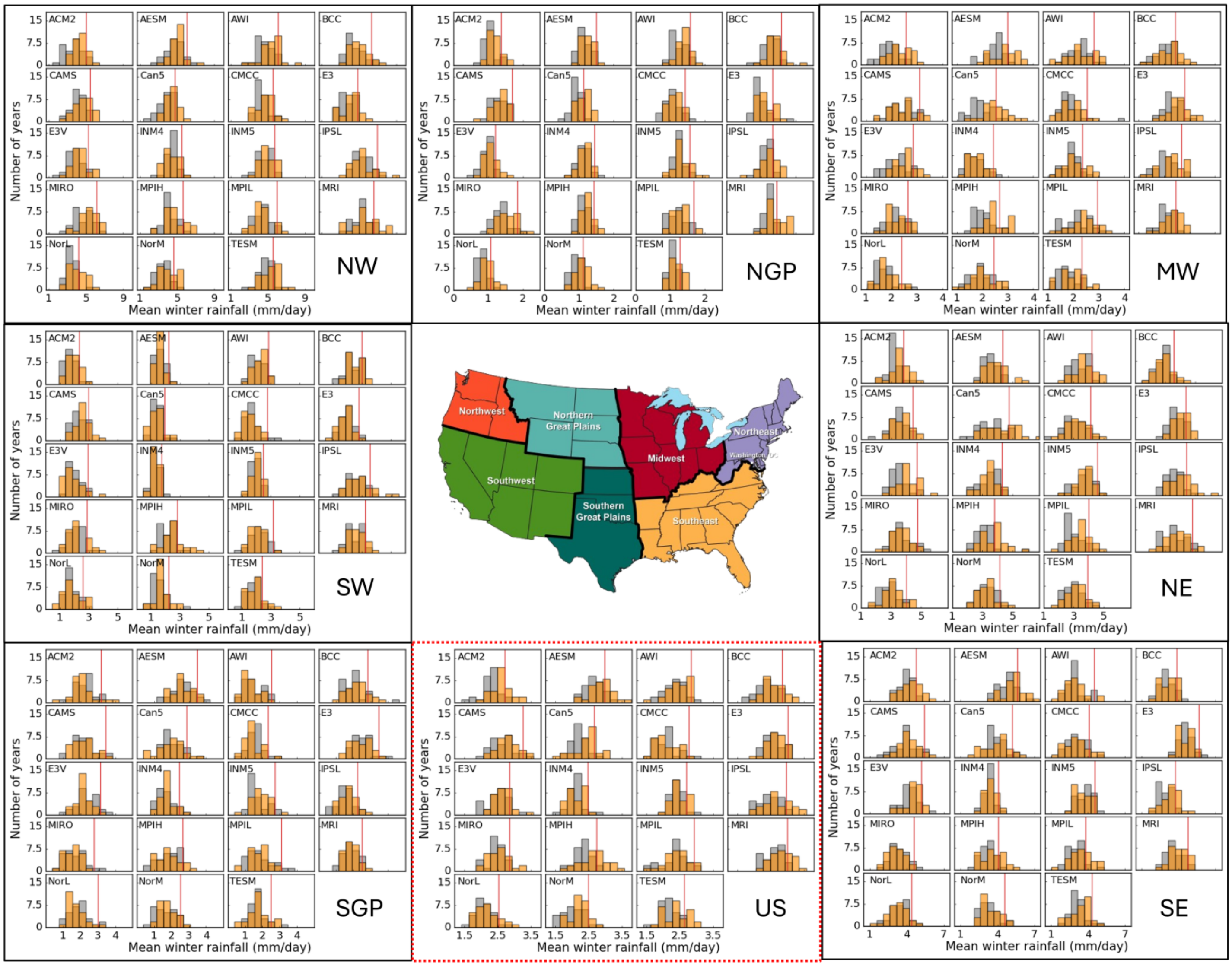

Figure S8. Mean winter precipitation (mm/day) over all of the US and seven subregions between the historical period (1985–2014) and future period (2070–2099) under SSP2–4.5. The historical (future) precipitation distribution is represented in gray (orange). The vertical red line represents the 95th percentile of 1985–2014. The spatial plot in the middle is the study domain, showing the seven CONUS subregions.

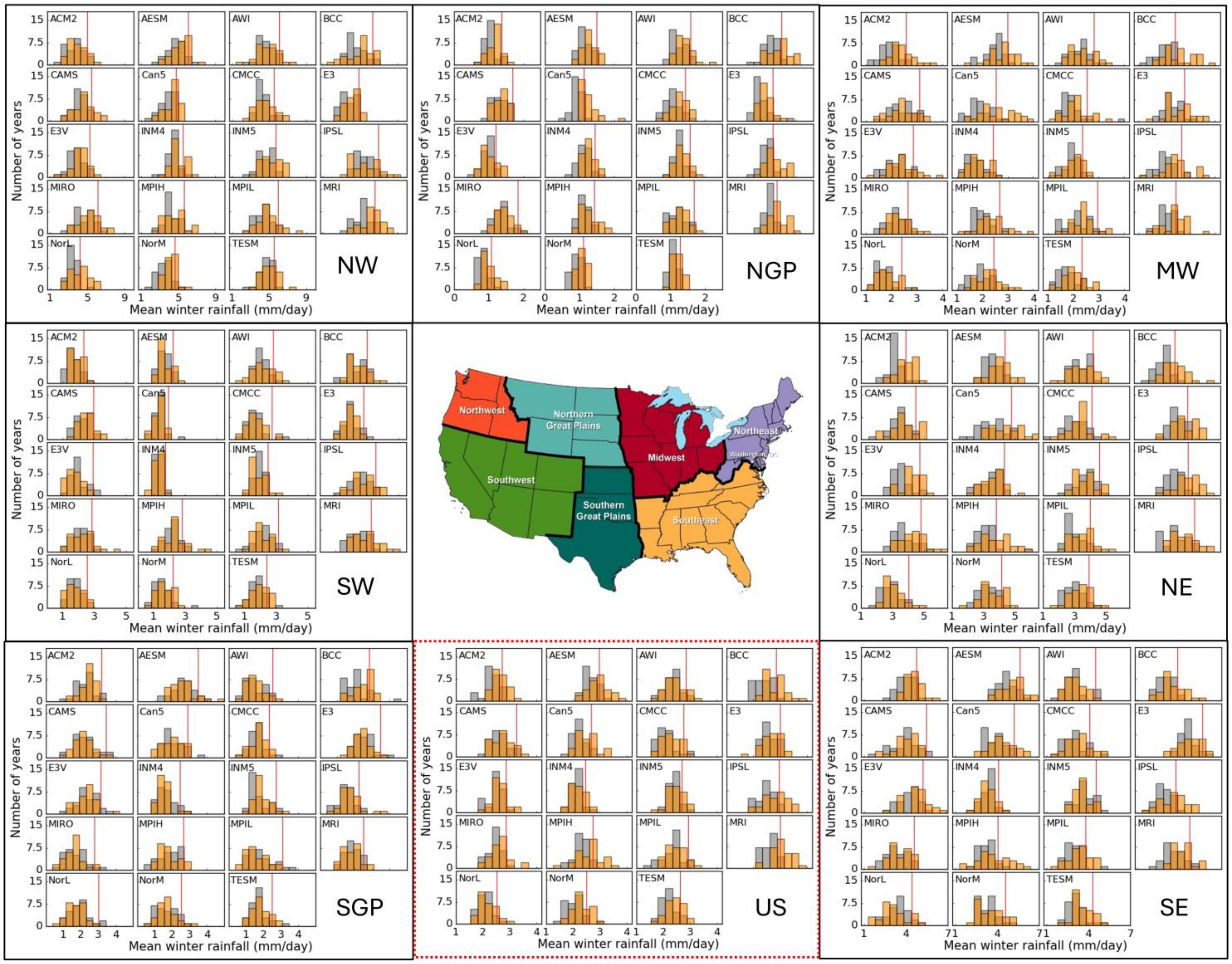

Figure S9. Mean winter precipitation (mm/day) over all of the US and seven subregions between the historical period (1985–2014) and future period (2070–2099) under SSP3–7.0. The historical (future) precipitation distribution is represented in gray (orange). The vertical red line represents the 95th percentile of 1985–2014. The spatial plot in the middle is the study domain, showing the seven CONUS subregions.

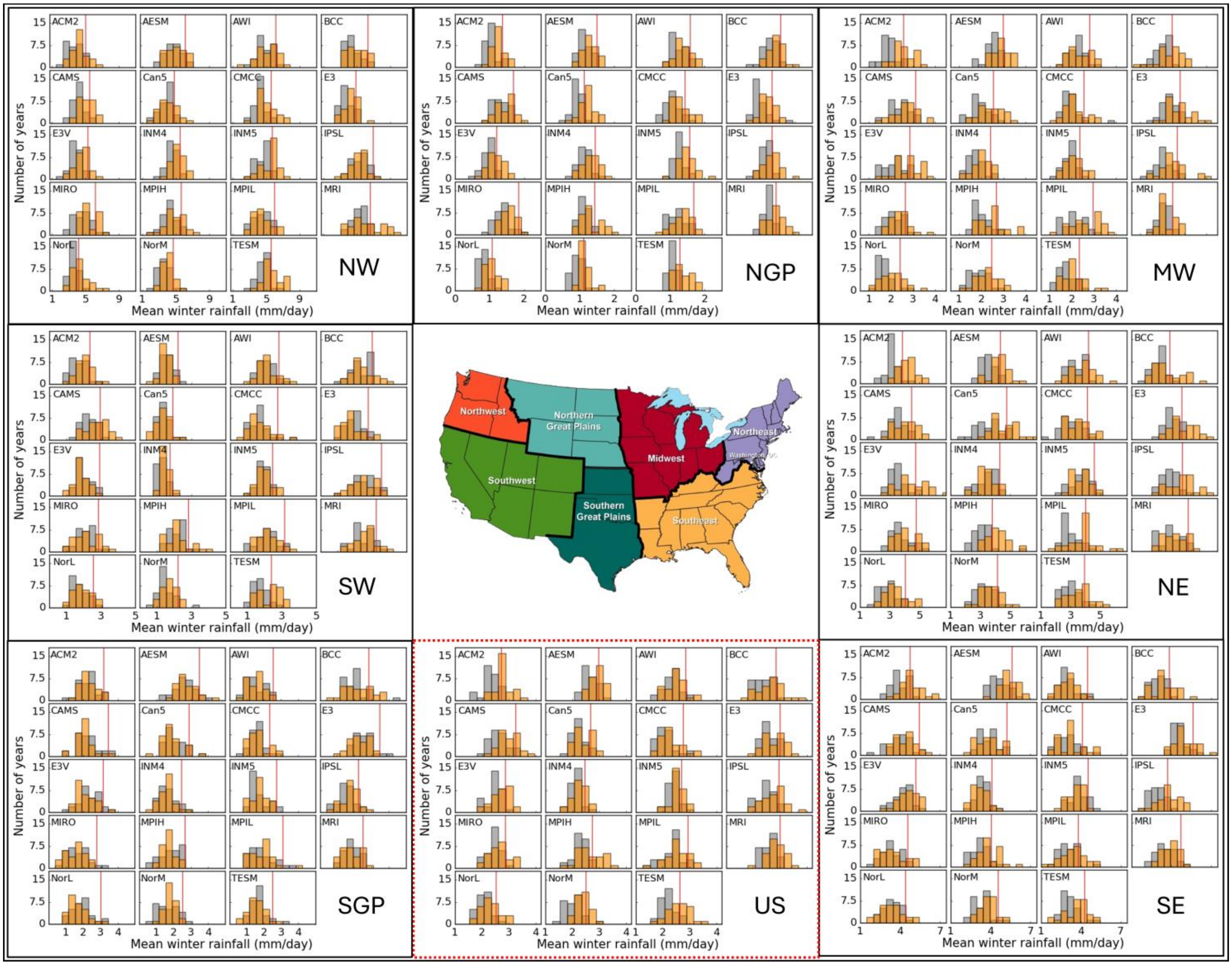

Figure S10. Mean winter precipitation (mm/day) over all of the US and seven subregions between the historical period (1985–2014) and future period (2070–2099) under SSP5–8.5. The historical (future) precipitation distribution is represented in gray (orange). The vertical red line represents the 95th percentile of 1985–2014. The spatial plot in the middle is the study domain, showing the seven CONUS subregions.

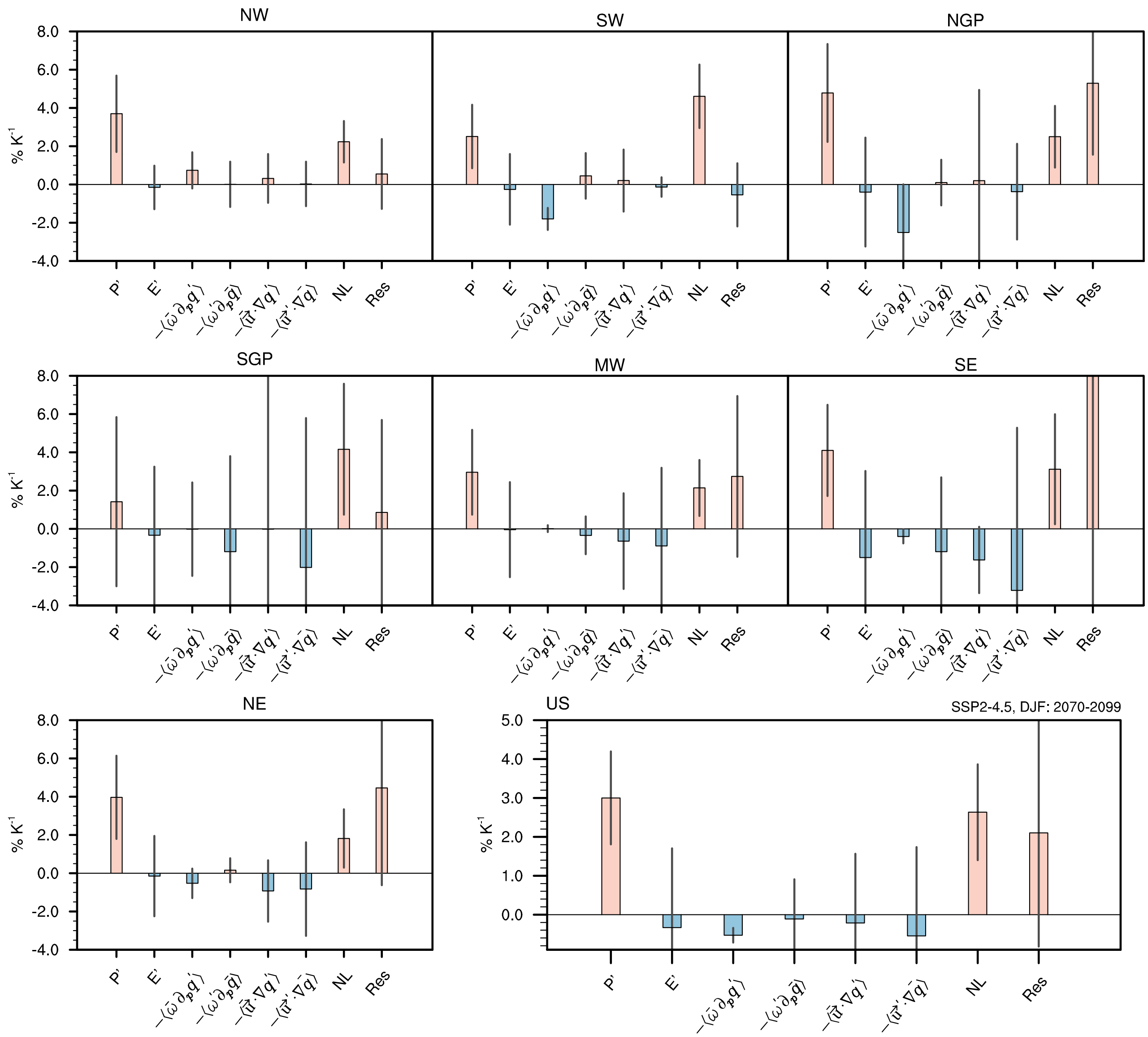

Figure S11. Projected changes in moisture budget terms in the long term (2070–2099; under the SSP2-4.5 scenario) averaged over all of the US and seven subregions relative to 1985–2014. The bars represent EnsMean, while the vertical line denotes the plus/minus one-time STD, which is based on the spread across models. All terms are scaled by the area-mean warming over the subregions. Unit: %/K. Six CMIP6 models (CAMS-CSM-1.0, EC-Earth3, EC-Earth-Veg, IPSL-CM6A-LR, MIROC6, and MRI-ESM2-0) are used for the computation of this figure.

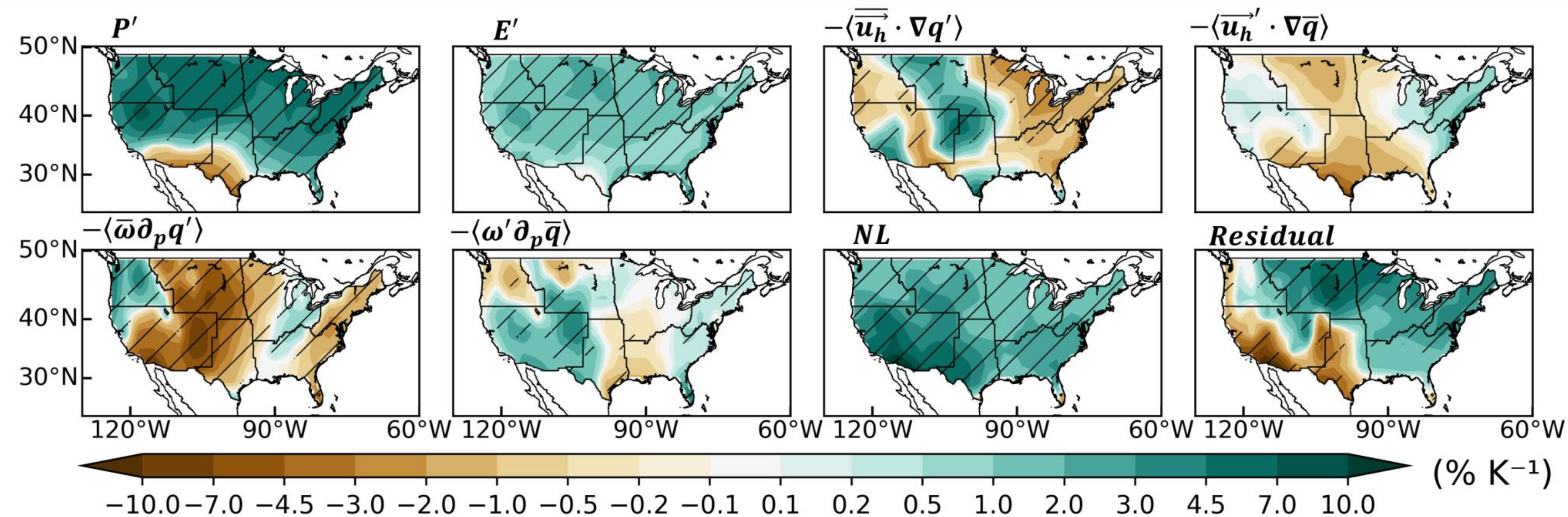

Figure S12. Spatial changes in mean winter moisture budget terms (2070–2099 relative to 1985–2014) scaled with mean temperature change (% K^{-1}) under SSP5–8.5. Hatching indicates grid points where at least 70% of the models agree on the sign of EnsMean.

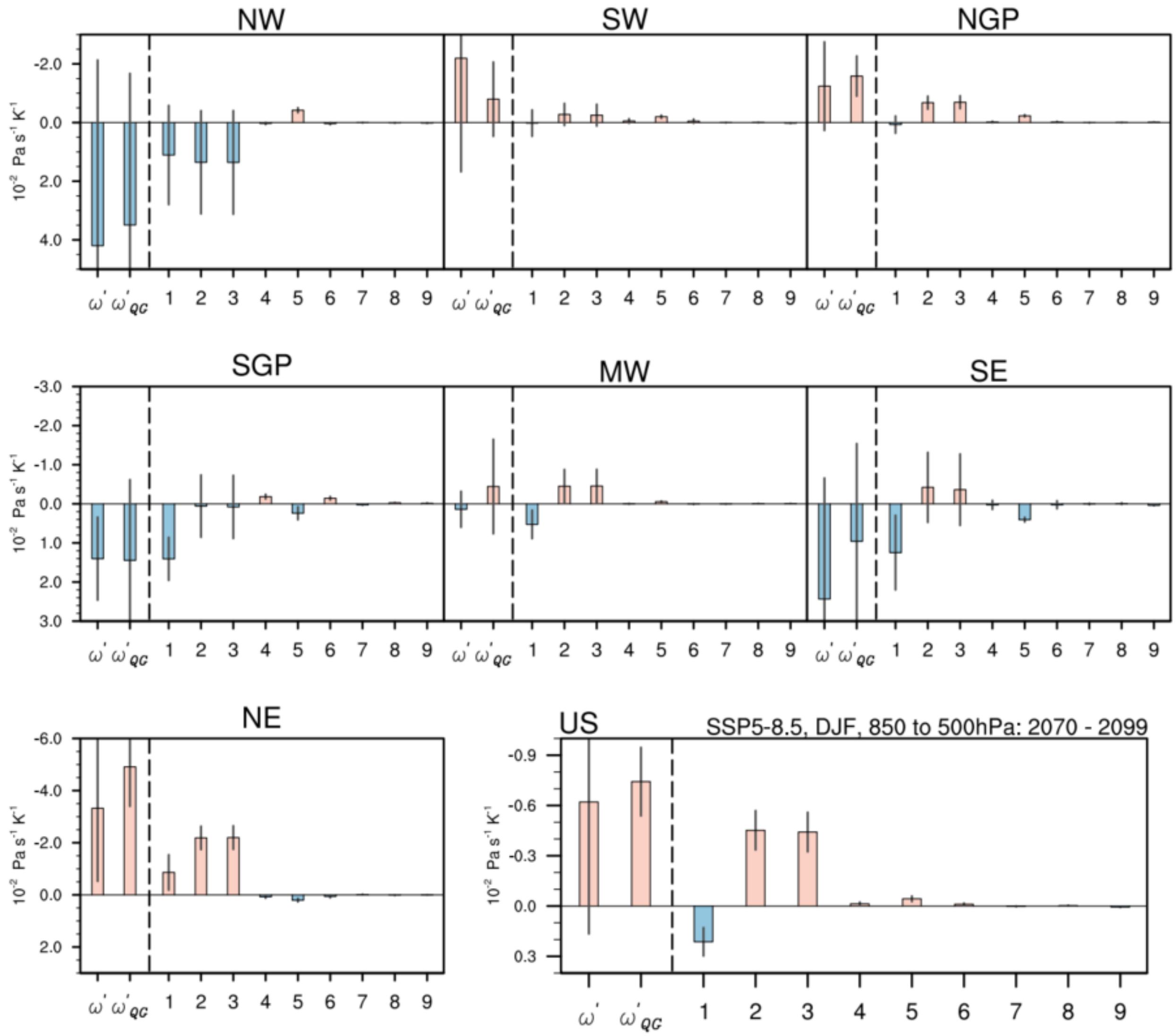

Figure S13. Projected changes in quasi-geostrophic omega terms in the long term (2070–2099; under the SSP5-8.5 scenario) averaged over all of the US and seven subregions relative to 1985–2014. The bars represent EnsMean, while the vertical line denotes the plus/minus one-time STD, which is based on the spread across models. All terms are scaled by the area-mean warming over the subregions. Unit: 10^{-2} Pa s^{-1} K^{-1}. The values on the y-axis have been reversed ($-1.0 \times$ Pa s^{-1}).

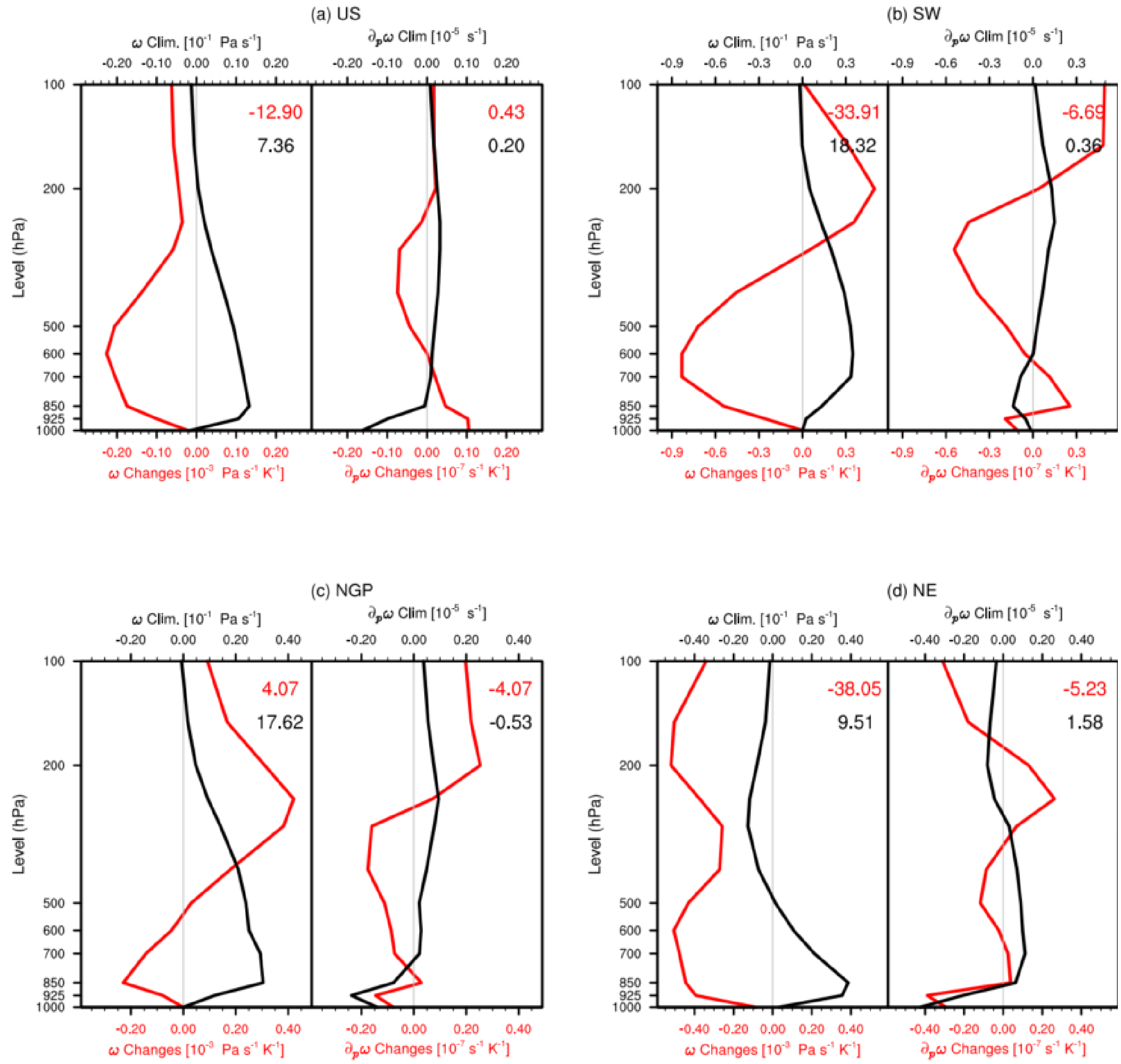

Figure S14. Vertical profile of mean DJF vertical velocity for selected subregions where enhancement of ω' is strongly associated with projected winter precipitation increase. Black (red) lines represent present-day climatology (projected changes).

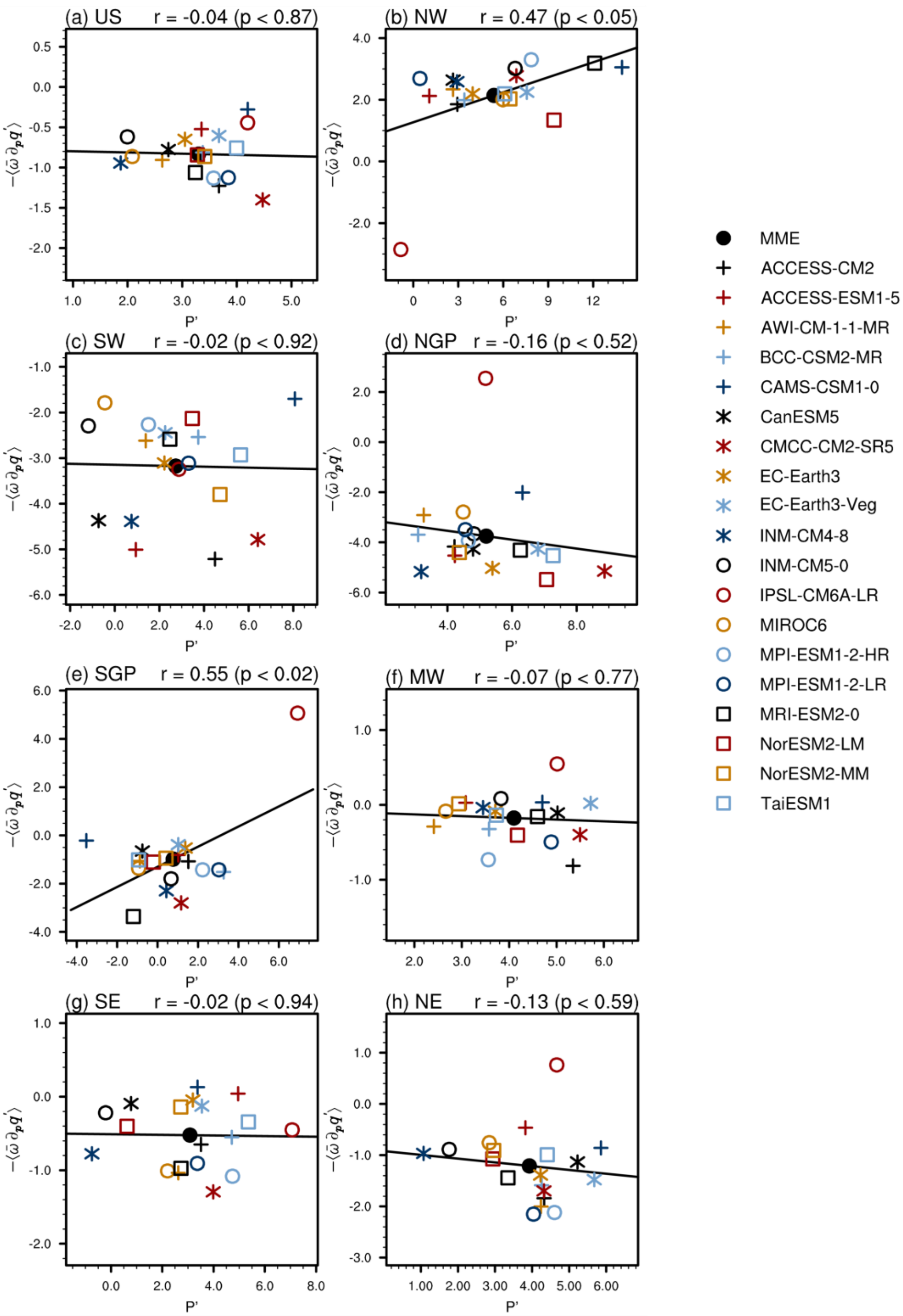

Figure S15. Relationship between winter precipitation changes and $-\langle\overline{\omega}\partial_p q'\rangle$ over all of the US and seven subregions under the SSP5–8.5 scenario. The solid lines indicate a linear fit, with the correlation coefficient and p-value shown at the top. Unit: %/K.

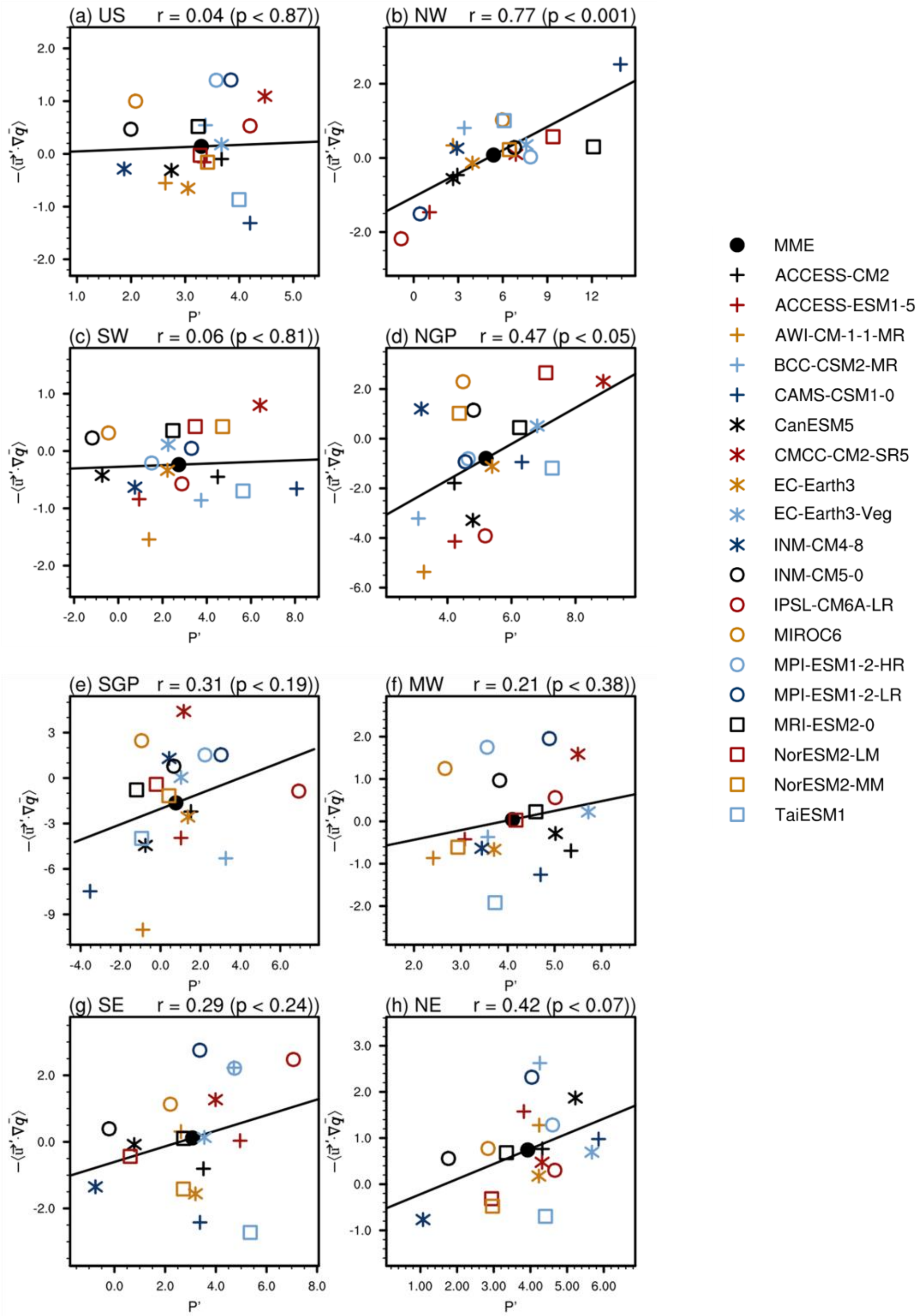

Figure S16. Relationship between winter precipitation changes and $-\langle \overrightarrow{u_h}' \cdot \nabla \bar{q} \rangle$ over all of the US and seven subregions under the SSP5–8.5 scenario. The solid lines indicate a linear fit, with the correlation coefficient and p-value shown at the top. Unit: %/K.

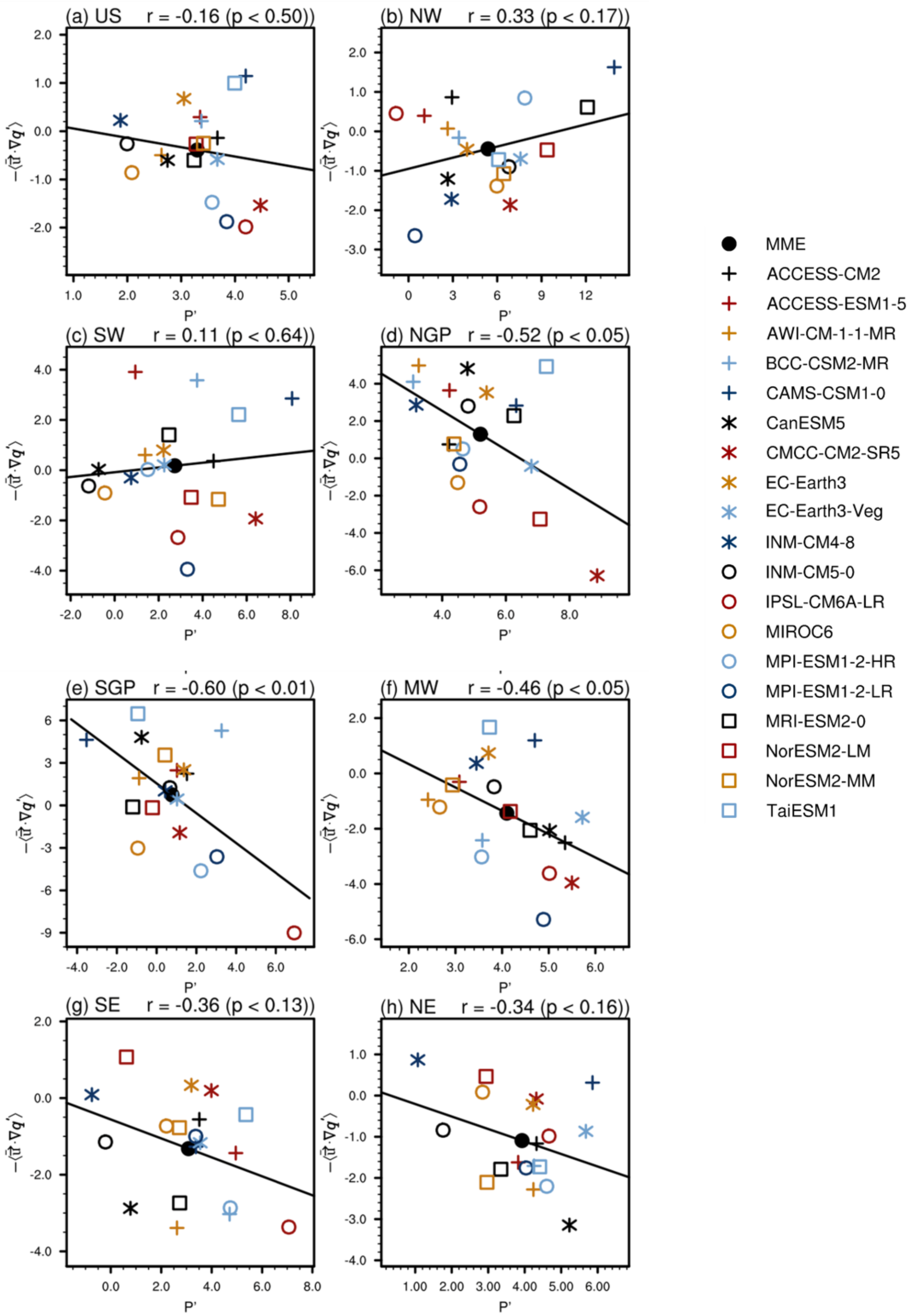

Figure S17. Relationship between winter precipitation changes and $-\langle\overrightarrow{u_h}\cdot\nabla q'\rangle$ over all of the US and seven subregions under the SSP5–8.5 scenario. The solid lines indicate a linear fit, with the correlation coefficient and p-value shown at the top. Unit: %/K.

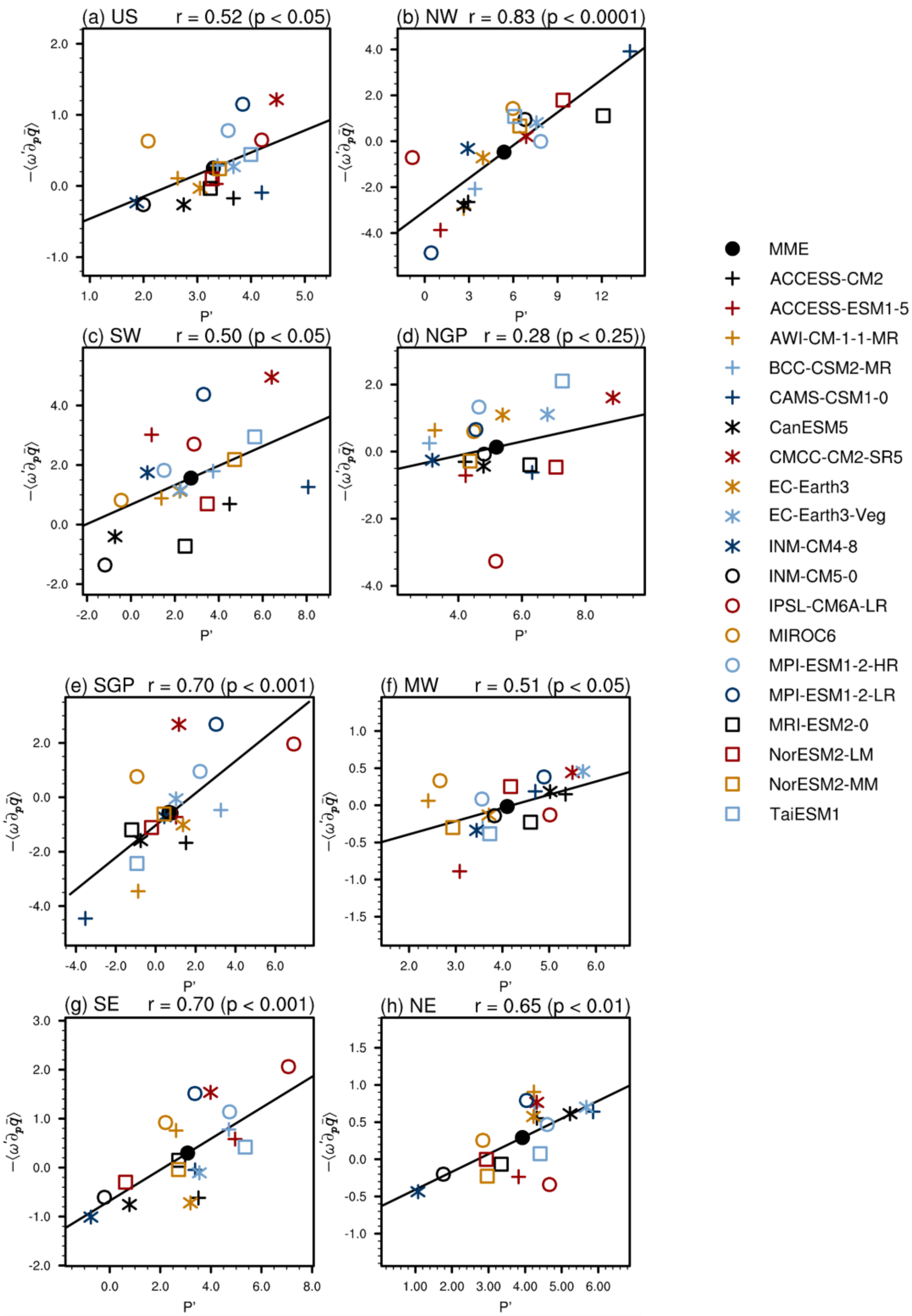

Figure S18. Relationship between winter precipitation changes and $-\langle\omega'\partial_p\bar{q}\rangle$ over all of the US and seven subregions under the SSP5–8.5 scenario. The solid lines indicate a linear fit, with the correlation coefficient and p-value shown at the top. Unit: %/K.

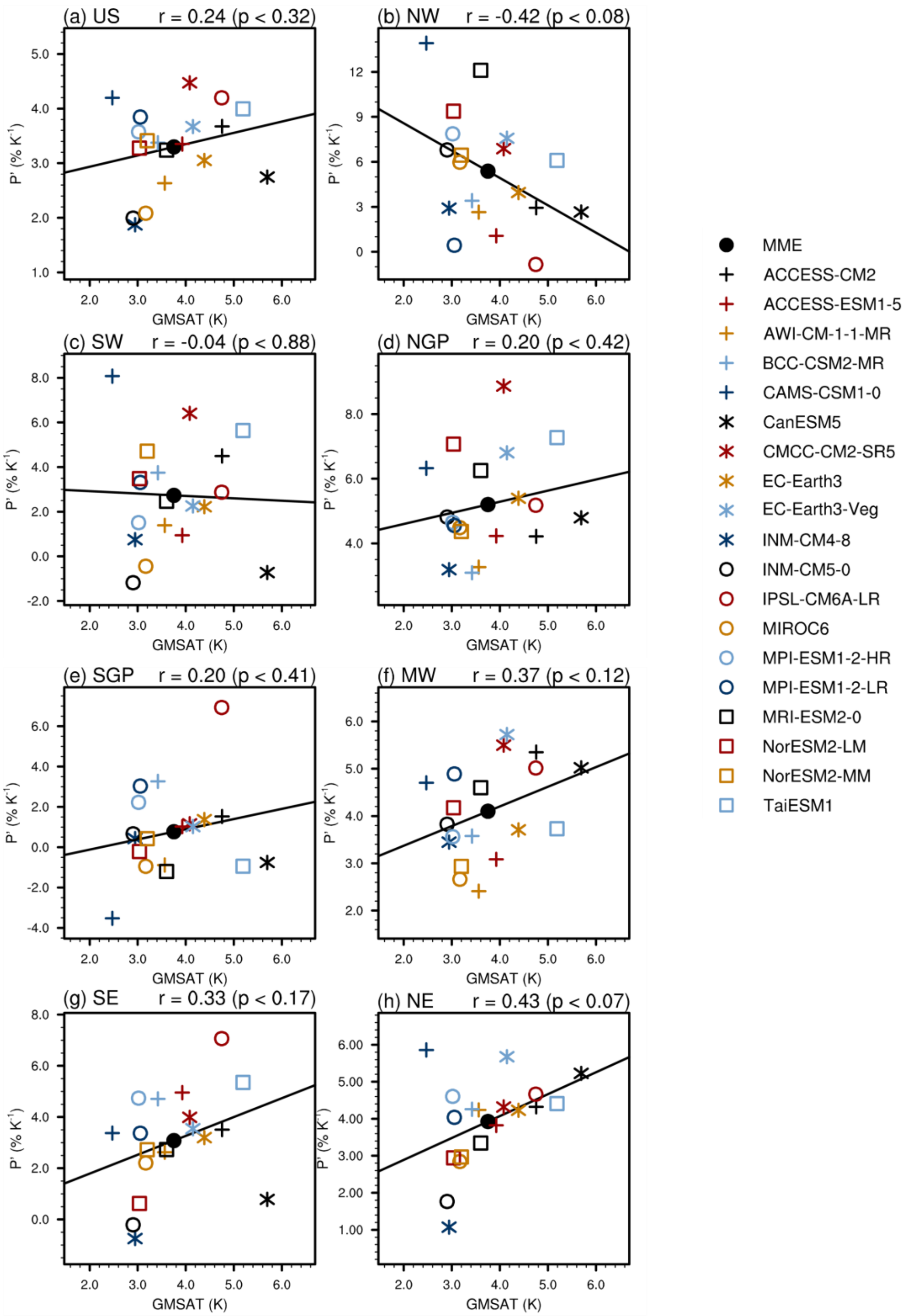

Figure S19. Relationship between global mean surface air temperature (GMSAT) changes and winter precipitation changes over all of the US and seven subregions under the SSP5–8.5 scenario. The solid lines indicate a linear fit, with the correlation coefficient and p-value shown at the top. Unit: K to GMSAT and %/K to P′.

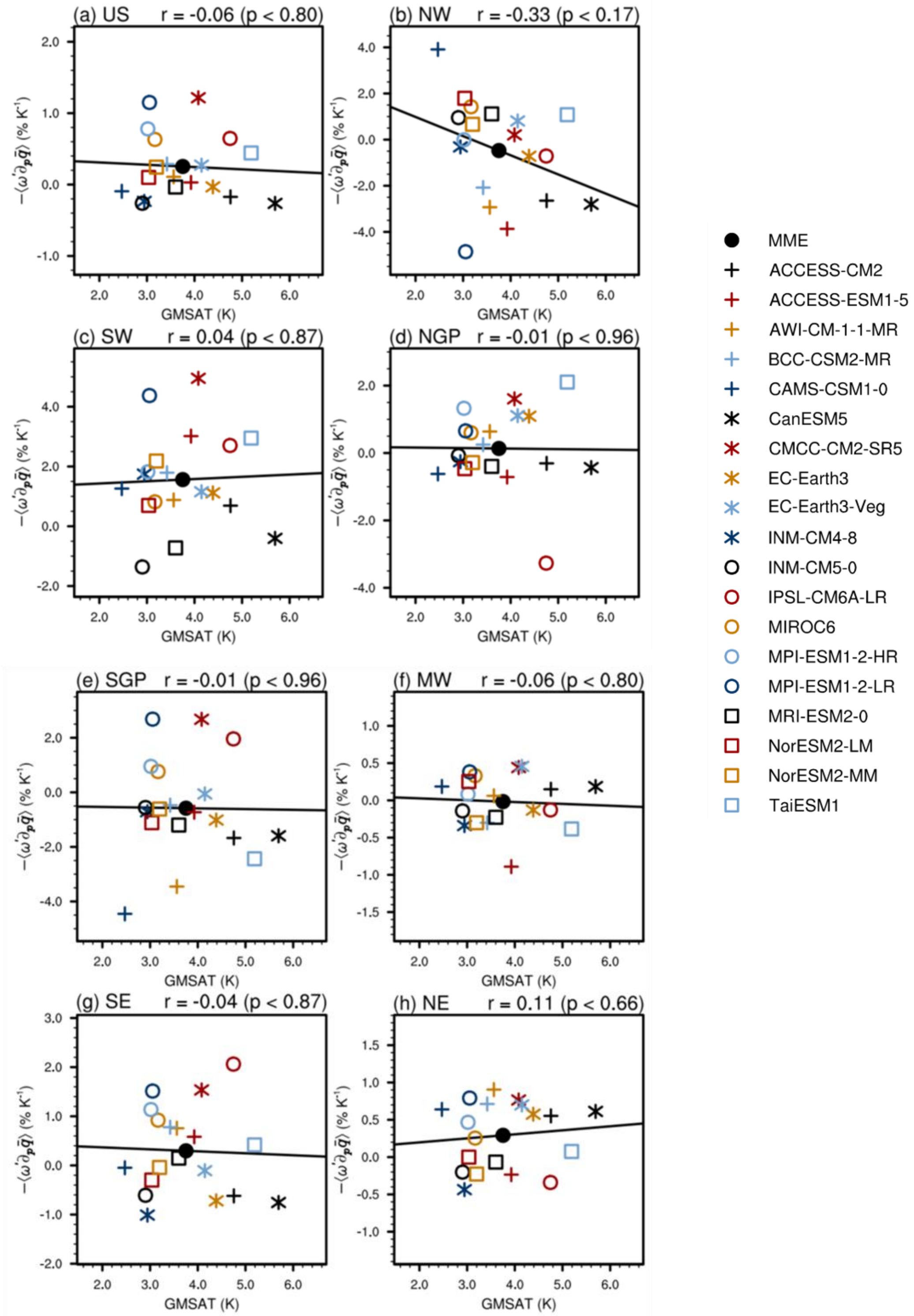

Figure S20. Relationship between global mean surface air temperature (GMSAT) changes and $-\langle \omega' \partial_p \bar{q} \rangle$ over all of the US and seven subregions under the SSP5–8.5 scenario. The solid lines indicate a linear fit, with the correlation coefficient and p-value shown at the top. Unit: K to GMSAT and %/K to $-\langle \omega' \partial_p \bar{q} \rangle$.

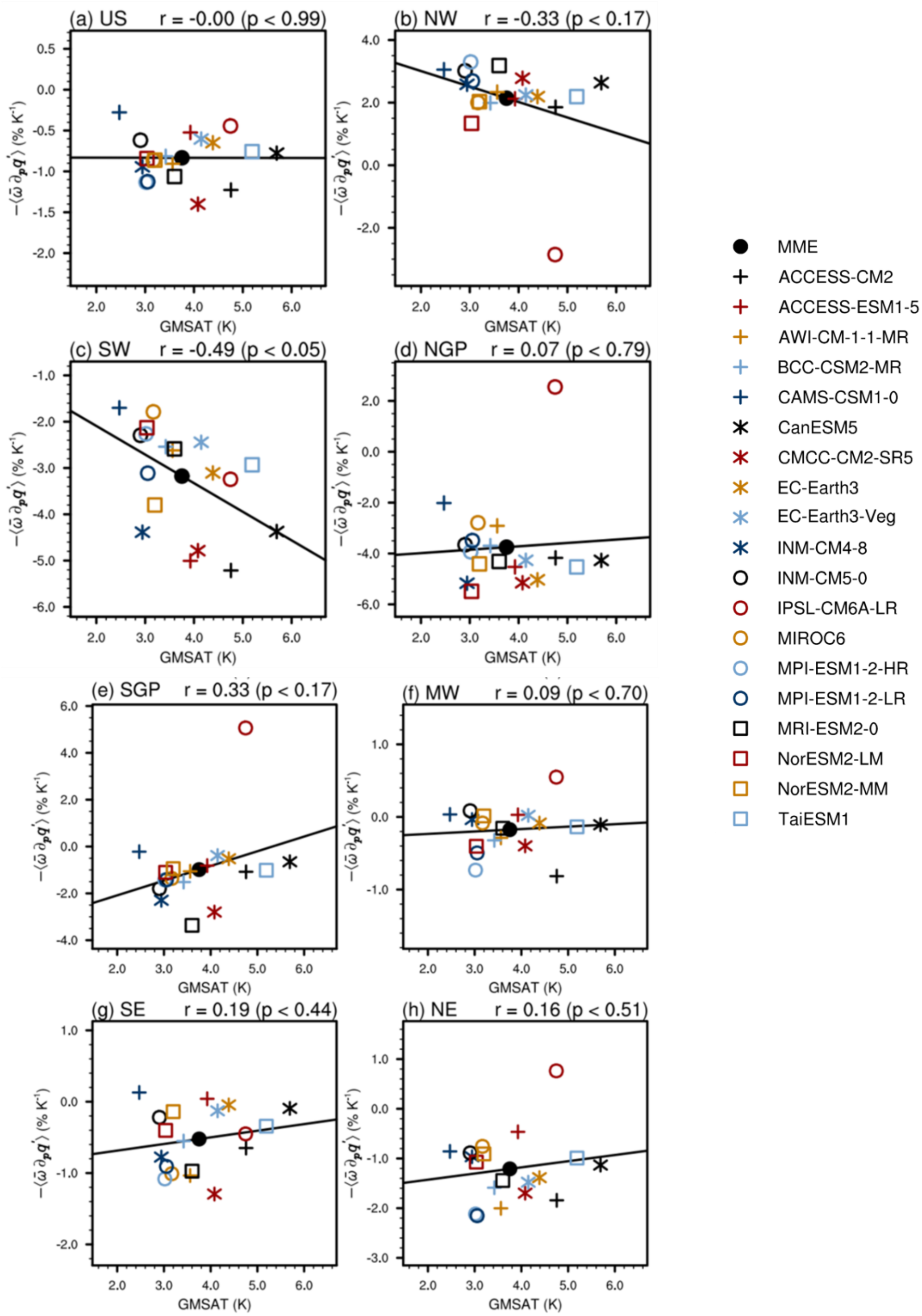

Figure S21. Relationship between global mean surface air temperature (GMSAT) changes and $-\langle\overline{\omega}\partial_p q'\rangle$ over all of the US and seven subregions under the SSP5–8.5 scenario. The solid lines indicate a linear fit, with the correlation coefficient and p-value shown at the top. Unit: K to GMSAT and %/K to $-\langle\overline{\omega}\partial_p q'\rangle$.

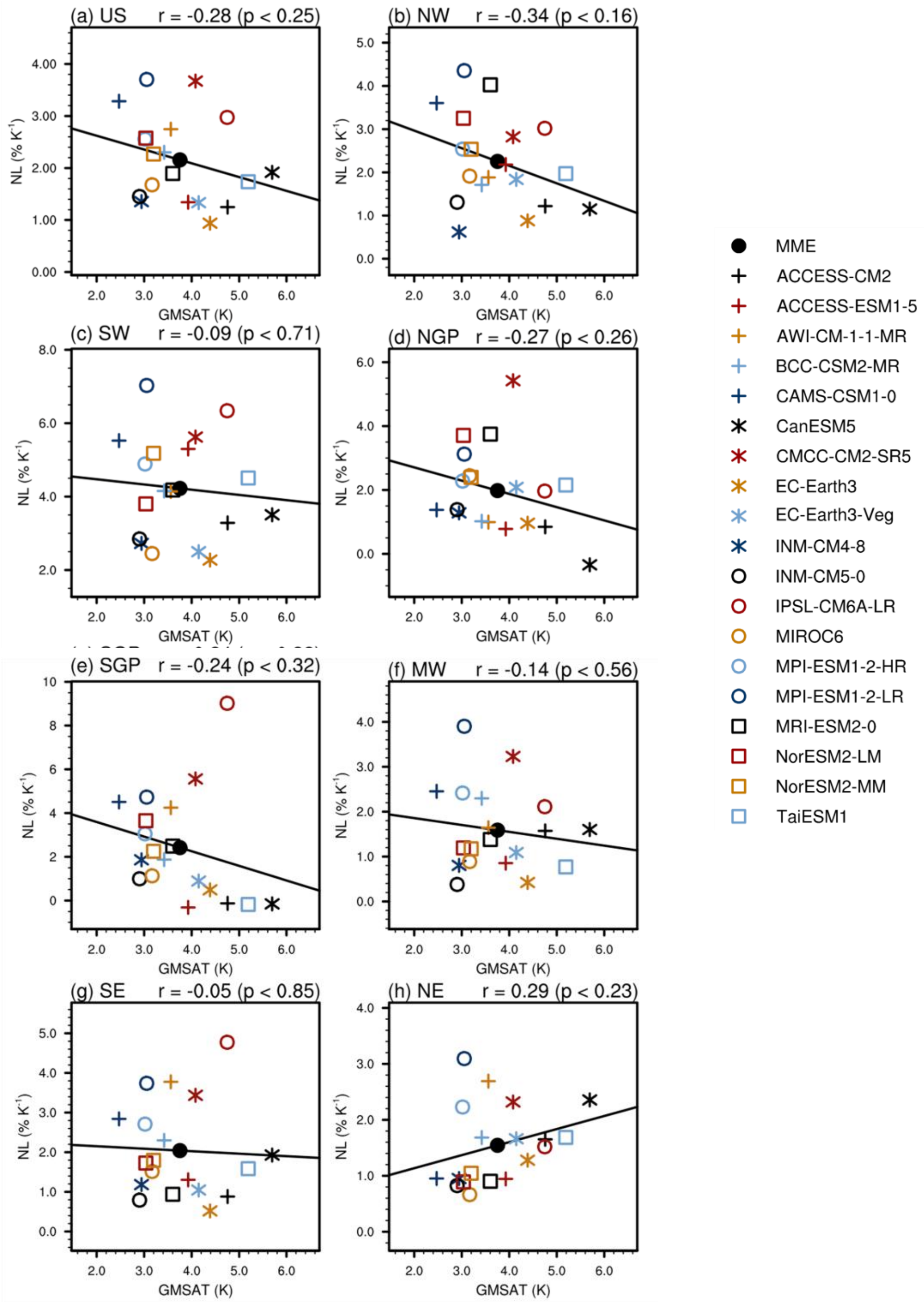

Figure S22. Relationship between global mean surface air temperature (GMSAT) changes and NL over all of the US and seven subregions under the SSP5–8.5 scenario. The solid lines indicate a linear fit, with the correlation coefficient and p-value shown at the top. Unit: K to GMSAT and %/K to NL.

References

1. Hawkins, E. & Sutton, R. The potential to narrow uncertainty in projections of regional precipitation change. *Clim Dyn* **37**, 407–418 (2011).
2. Hawkins, E. & Sutton, R. The Potential to Narrow Uncertainty in Regional Climate Predictions. *Bull. Amer. Meteor. Soc.* **90**, 1095–1108 (2009).
3. Dix, M. et al. CSIRO-ARCCSS ACCESS-CM2 model output prepared for CMIP6 CMIP historical. Earth System Grid Federation; 10.22033/ESGF/CMIP6.4271 (2019).
4. Dix, M. et al. CSIRO-ARCCSS ACCESS-CM2 model output prepared for CMIP6 ScenarioMIP ssp245. Earth System Grid Federation; 10.22033/ESGF/CMIP6.4321 (2019).
5. Dix, M. et al. CSIRO-ARCCSS ACCESS-CM2 model output prepared for CMIP6 ScenarioMIP ssp370. Earth System Grid Federation; 10.22033/ESGF/CMIP6.4323 (2019).
6. Dix, M. et al. CSIRO-ARCCSS ACCESS-CM2 model output prepared for CMIP6 ScenarioMIP ssp585. Earth System Grid Federation; 10.22033/ESGF/CMIP6.4332 (2019).
7. Ziehn, T. et al. CSIRO ACCESS-ESM1.5 model output prepared for CMIP6 CMIP historical. Earth System Grid Federation; 10.22033/ESGF/CMIP6.4272 (2019).
8. Ziehn, T. et al. CSIRO ACCESS-ESM1.5 model output prepared for CMIP6 ScenarioMIP ssp245. Earth System Grid Federation; 10.22033/ESGF/CMIP6.4322 (2019).
9. Ziehn, T. et al. CSIRO ACCESS-ESM1.5 model output prepared for CMIP6 ScenarioMIP ssp370. Earth System Grid Federation; 10.22033/ESGF/CMIP6.4324 (2019).
10. Ziehn, T. et al. CSIRO ACCESS-ESM1.5 model output prepared for CMIP6 ScenarioMIP ssp585. Earth System Grid Federation; 10.22033/ESGF/CMIP6.4333 (2019).
11. Semmler, T. et al. AWI AWI-CM1.1MR model output prepared for CMIP6 CMIP historical. Earth System Grid Federation; 10.22033/ESGF/CMIP6.2686 (2018).

12. Semmler, T. et al. AWI AWI-CM1.1MR model output prepared for CMIP6 ScenarioMIP ssp245. Earth System Grid Federation; 10.22033/ESGF/CMIP6.2800 (2018).
13. Semmler, T. et al. AWI AWI-CM1.1MR model output prepared for CMIP6 ScenarioMIP ssp370. Earth System Grid Federation; 10.22033/ESGF/CMIP6.2803 (2019).
14. Semmler, T. et al. AWI AWI-CM1.1MR model output prepared for CMIP6 ScenarioMIP ssp585. Earth System Grid Federation; 10.22033/ESGF/CMIP6.2817 (2019).
15. Wu, T. et al. BCC BCC-CSM2MR model output prepared for CMIP6 CMIP historical. Earth System Grid Federation; 10.22033/ESGF/CMIP6.2948 (2018).
16. Xin, X. et al. BCC BCC-CSM2MR model output prepared for CMIP6 ScenarioMIP ssp245. Earth System Grid Federation; 10.22033/ESGF/CMIP6.3030 (2019).
17. Xin, X. et al. BCC BCC-CSM2MR model output prepared for CMIP6 ScenarioMIP ssp370. Earth System Grid Federation; 10.22033/ESGF/CMIP6.3035 (2019).
18. Xin, X. et al. BCC BCC-CSM2MR model output prepared for CMIP6 ScenarioMIP ssp585. Earth System Grid Federation; 10.22033/ESGF/CMIP6.3050 (2019).
19. Rong, X. CAMS CAMS_CSM1.0 model output prepared for CMIP6 CMIP historical. Earth System Grid Federation; 10.22033/ESGF/CMIP6.9754 (2019).
20. Rong, X. CAMS CAMS-CSM1.0 model output prepared for CMIP6 ScenarioMIP ssp245. Earth System Grid Federation; 10.22033/ESGF/CMIP6.11047 (2019).
21. Rong, X. CAMS CAMS-CSM1.0 model output prepared for CMIP6 ScenarioMIP ssp370. Earth System Grid Federation; 10.22033/ESGF/CMIP6.11048 (2019).
22. Rong, X. CAMS CAMS-CSM1.0 model output prepared for CMIP6 ScenarioMIP ssp585. Earth System Grid Federation; 10.22033/ESGF/CMIP6.11052 (2019).

23. Swart, N. C. et al. CCCma CanESM5 model output prepared for CMIP6 CMIP historical. Earth System Grid Federation; 10.22033/ESGF/CMIP6.3610 (2019).
24. Swart, N. C. et al. CCCma CanESM5 model output prepared for CMIP6 ScenarioMIP ssp245. Earth System Grid Federation; 10.22033/ESGF/CMIP6.3685 (2019).
25. Swart, N. C. et al. CCCma CanESM5 model output prepared for CMIP6 ScenarioMIP ssp370. Earth System Grid Federation; 10.22033/ESGF/CMIP6.3690 (2019).
26. Swart, N. C. et al. CCCma CanESM5 model output prepared for CMIP6 ScenarioMIP ssp585. Earth System Grid Federation; 10.22033/ESGF/CMIP6.3696 (2019).
27. Lovato, T. & Peano, D. CMCC CMCC-CM2-SR5 model output prepared for CMIP6 CMIP historical. Earth System Grid Federation; 10.22033/ESGF/CMIP6.3825 (2020).
28. Lovato, T. & Peano, D. CMCC CMCC-CM2-SR5 model output prepared for CMIP6 ScenarioMIP ssp245. Earth System Grid Federation; 10.22033/ESGF/CMIP6.3889 (2020).
29. Lovato, T. & Peano, D. CMCC CMCC-CM2-SR5 model output prepared for CMIP6 ScenarioMIP ssp370. Earth System Grid Federation; 10.22033/ESGF/CMIP6.3890 (2020).
30. Lovato, T. & Peano, D. CMCC CMCC-CM2-SR5 model output prepared for CMIP6 ScenarioMIP ssp585. Earth System Grid Federation; 10.22033/ESGF/CMIP6.3896 (2020).
31. EC-Earth Consortium (EC-Earth). EC-Earth-Consortium EC-Earth3 model output prepared for CMIP6 CMIP historical. Earth System Grid Federation; 10.22033/ESGF/CMIP6.4700 (2019).
32. EC-Earth Consortium (EC-Earth). EC-Earth-Consortium EC-Earth3 model output prepared for CMIP6 ScenarioMIP ssp245. Earth System Grid Federation; 10.22033/ESGF/CMIP6.4880 (2019).

33. EC-Earth Consortium (EC-Earth). EC-Earth-Consortium EC-Earth3 model output prepared for CMIP6 ScenarioMIP ssp370. Earth System Grid Federation; 10.22033/ESGF/CMIP6.4884 (2019).

34. EC-Earth Consortium (EC-Earth). EC-Earth-Consortium EC-Earth3 model output prepared for CMIP6 ScenarioMIP ssp585. Earth System Grid Federation; 10.22033/ESGF/CMIP6.4912 (2019).

35. EC-Earth Consortium (EC-Earth). EC-Earth-Consortium EC-Earth3-Veg model output prepared for CMIP6 CMIP historical. Earth System Grid Federation; 10.22033/ESGF/CMIP6.4706 (2019).

36. EC-Earth Consortium (EC-Earth). EC-Earth-Consortium EC-Earth3-Veg model output prepared for CMIP6 ScenarioMIP ssp245. Earth System Grid Federation; 10.22033/ESGF/CMIP6.4882 (2019).

37. EC-Earth Consortium (EC-Earth). EC-Earth-Consortium EC-Earth3-Veg model output prepared for CMIP6 ScenarioMIP ssp370. Earth System Grid Federation; 10.22033/ESGF/CMIP6.4886 (2019).

38. EC-Earth Consortium (EC-Earth). EC-Earth-Consortium EC-Earth3-Veg model output prepared for CMIP6 ScenarioMIP ssp585. Earth System Grid Federation; 10.22033/ESGF/CMIP6.4914 (2019).

39. Volodin, E. et al. INM INM-CM4-8 model output prepared for CMIP6 CMIP historical. Earth System Grid Federation; 10.22033/ESGF/CMIP6.5069 (2019).

40. Volodin, E. et al. INM INM-CM4-8 model output prepared for CMIP6 ScenarioMIP ssp245. Earth System Grid Federation; 10.22033/ESGF/CMIP6.12327 (2019).

41. Volodin, E. et al. INM INM-CM4-8 model output prepared for CMIP6 ScenarioMIP ssp370. Earth System Grid Federation; 10.22033/ESGF/CMIP6.12329 (2019).

42. Volodin, E. et al. INM INM-CM4-8 model output prepared for CMIP6 ScenarioMIP ssp585. Earth System Grid Federation; 10.22033/ESGF/CMIP6.12337 (2019).

43. Volodin, E. et al. INM INM-CM5-0 model output prepared for CMIP6 CMIP historical. Earth System Grid Federation; 10.22033/ESGF/CMIP6.5070 (2019).

44. Volodin, E. et al. INM INM-CM5-0 model output prepared for CMIP6 ScenarioMIP ssp245. Earth System Grid Federation; 10.22033/ESGF/CMIP6.12328 (2019).

45. Volodin, E. et al. INM INM-CM5-0 model output prepared for CMIP6 ScenarioMIP ssp370. Earth System Grid Federation; 10.22033/ESGF/CMIP6.12330 (2019).

46. Volodin, E. et al. INM INM-CM5-0 model output prepared for CMIP6 ScenarioMIP ssp585. Earth System Grid Federation; 10.22033/ESGF/CMIP6.12338 (2019).

47. Boucher, O. et al. IPSL IPSL-CM6A-LR model output prepared for CMIP6 CMIP historical. Earth System Grid Federation; 10.22033/ESGF/CMIP6.5195 (2018).

48. Boucher, O. et al. IPSL IPSL-CM6A-LR model output prepared for CMIP6 ScenarioMIP ssp245. Earth System Grid Federation; 10.22033/ESGF/CMIP6.5264 (2019).

49. Boucher, O. et al. IPSL IPSL-CM6A-LR model output prepared for CMIP6 ScenarioMIP ssp370. Earth System Grid Federation; 10.22033/ESGF/CMIP6.5265 (2019).

50. Boucher, O. et al. IPSL IPSL-CM6A-LR model output prepared for CMIP6 ScenarioMIP ssp585. Earth System Grid Federation; 10.22033/ESGF/CMIP6.5271 (2019).

51. Tatebe, H. & Watanabe, M. MIROC MIROC6 model output prepared for CMIP6 CMIP historical. Earth System Grid Federation; 10.22033/ESGF/CMIP6.5603 (2018).

52. Shiogama, H., Abe, M. & Tatebe, H. MIROC MIROC6 model output prepared for CMIP6 ScenarioMIP ssp245. Earth System Grid Federation; 10.22033/ESGF/CMIP6.5746 (2019).

53. Shiogama, H., Abe, M. & Tatebe, H. MIROC MIROC6 model output prepared for CMIP6 ScenarioMIP ssp370. Earth System Grid Federation; 10.22033/ESGF/CMIP6.5752 (2019).

54. Shiogama, H., Abe, M. & Tatebe, H. MIROC MIROC6 model output prepared for CMIP6 ScenarioMIP ssp585. Earth System Grid Federation; 10.22033/ESGF/CMIP6.5771 (2019).

55. Jungclaus, J. et al. MPI-M MPI-ESM1.2-HR model output prepared for CMIP6 CMIP historical. Earth System Grid Federation; 10.22033/ESGF/CMIP6.6594 (2019).

56. Schupfner, M. et al. DKRZ MPI-ESM1.2-HR model output prepared for CMIP6 ScenarioMIP ssp245. Earth System Grid Federation; 10.22033/ESGF/CMIP6.4398 (2019).

57. Schupfner, M. et al. DKRZ MPI-ESM1.2-HR model output prepared for CMIP6 ScenarioMIP ssp370. Earth System Grid Federation; 10.22033/ESGF/CMIP6.4399 (2019).

58. Schupfner, M. et al. DKRZ MPI-ESM1.2-HR model output prepared for CMIP6 ScenarioMIP ssp585. Earth System Grid Federation; 10.22033/ESGF/CMIP6.4403 (2019).

59. Wieners, K.-H. et al. MPI-M MPI-ESM1.2-LR model output prepared for CMIP6 CMIP historical. Earth System Grid Federation; 10.22033/ESGF/CMIP6.6595 (2019).

60. Wieners, K.-H. et al. MPI-M MPI-ESM1.2-LR model output prepared for CMIP6 ScenarioMIP ssp245. Earth System Grid Federation; 10.22033/ESGF/CMIP6.6693 (2019).

61. Wieners, K.-H. et al. MPI-M MPI-ESM1.2-LR model output prepared for CMIP6 ScenarioMIP ssp370. Earth System Grid Federation; 10.22033/ESGF/CMIP6.6695 (2019).

62. Wieners, K.-H. et al. MPI-M MPI-ESM1.2-LR model output prepared for CMIP6 ScenarioMIP ssp585. Earth System Grid Federation; 10.22033/ESGF/CMIP6.6705 (2019).

63. Yukimoto, S. et al. MRI MRI-ESM2.0 model output prepared for CMIP6 CMIP historical. Earth System Grid Federation; 10.22033/ESGF/CMIP6.6842 (2019).
64. Yukimoto, S. et al. MRI MRI-ESM2.0 model output prepared for CMIP6 ScenarioMIP ssp245. Earth System Grid Federation; 10.22033/ESGF/CMIP6.6910 (2019).
65. Yukimoto, S. et al. MRI MRI-ESM2.0 model output prepared for CMIP6 ScenarioMIP ssp370. Earth System Grid Federation; 10.22033/ESGF/CMIP6.6915 (2019).
66. Yukimoto, S. et al. MRI MRI-ESM2.0 model output prepared for CMIP6 ScenarioMIP ssp585. Earth System Grid Federation; 10.22033/ESGF/CMIP6.6929 (2019).
67. Seland, Ø. et al. NCC NorESM2-LM model output prepared for CMIP6 CMIP historical. Earth System Grid Federation; 10.22033/ESGF/CMIP6.8036 (2019).
68. Seland, Ø. et al. NCC NorESM2-LM model output prepared for CMIP6 ScenarioMIP ssp245. Earth System Grid Federation; 10.22033/ESGF/CMIP6.8253 (2019).
69. Seland, Ø. et al. NCC NorESM2-LM model output prepared for CMIP6 ScenarioMIP ssp370. Earth System Grid Federation; 10.22033/ESGF/CMIP6.8268 (2019).
70. Seland, Ø. et al. NCC NorESM2-LM model output prepared for CMIP6 ScenarioMIP ssp585. Earth System Grid Federation; 10.22033/ESGF/CMIP6.8319 (2019).
71. Bentsen, M. et al. NCC NorESM2-MM model output prepared for CMIP6 CMIP historical. Earth System Grid Federation; 10.22033/ESGF/CMIP6.8040 (2019).
72. Bentsen, M. et al. NCC NorESM2-MM model output prepared for CMIP6 ScenarioMIP ssp245. Earth System Grid Federation; 10.22033/ESGF/CMIP6.8255 (2019).
73. Bentsen, M. et al. NCC NorESM2-MM model output prepared for CMIP6 ScenarioMIP ssp370. Earth System Grid Federation; 10.22033/ESGF/CMIP6.8270 (2019).

74. Bentsen, M. et al. NCC NorESM2-MM model output prepared for CMIP6 ScenarioMIP ssp585. Earth System Grid Federation; 10.22033/ESGF/CMIP6.8321 (2019).
75. Lee, W.-L. & Liang, H.-C. AS-RCEC TaiESM1.0 model output prepared for CMIP6 CMIP historical. Earth System Grid Federation; 10.22033/ESGF/CMIP6.9755 (2020).
76. Lee, W.-L. & Liang, H.-C. AS-RCEC TaiESM1.0 model output prepared for CMIP6 ScenarioMIP ssp245. Earth System Grid Federation; 10.22033/ESGF/CMIP6.9808 (2020).
77. Lee, W.-L. & Liang, H.-C. AS-RCEC TaiESM1.0 model output prepared for CMIP6 ScenarioMIP ssp370. Earth System Grid Federation; 10.22033/ESGF/CMIP6.9809 (2020).
78. Lee, W.-L. & Liang, H.-C. AS-RCEC TaiESM1.0 model output prepared for CMIP6 ScenarioMIP ssp585. Earth System Grid Federation; 10.22033/ESGF/CMIP6.9823 (2020).